iScience

CellPress
OPEN ACCESS

Review

Monitoring photovoltaic soiling: assessment, challenges, and perspectives of current and potential strategies

João Gabriel Bessa,[1] Leonardo Micheli,[1,*] Florencia Almonacid,[1] and Eduardo F. Fernández[1]

SUMMARY

Soiling is the process whereby dirt, dust, and organic/inorganic contaminants deposit on the surface of a photovoltaic (PV) module. It causes significant economic losses and can have a substantial impact on the expansion of photovoltaic technologies for energy generation. The first step to address soiling adequately is monitoring, as soiling mitigation has to be tailored to the specific conditions of each PV system and no universally valid strategy exists. The main focus of this study is to assess the current state of the art in soiling monitoring, in order to help the community better understand the needs and the challenges in this area. The potentials and the limitations of each monitoring method are discussed thoroughly in the paper, with the support of original experimental data. An estimation of the future soiling monitoring market trends is also presented, with a forecasted need for tens of thousands of new soiling monitors every year.

INTRODUCTION

Photovoltaic (PV) technologies directly convert sunlight into electricity and are one of the most diffused renewable energy sources. The 48% of the global net power capacity installed in 2019 was based on PV (Solar Power Europe, 2020). In addition, from the total 634 GW installed at the end of 2019, in the most conservative scenario, a capacity of at least 1,177 GW is expected to be installed worldwide by 2024, driven by the lower cost compared with nuclear, fossil, and other renewable sources (Solar Power Europe, 2020). In order to keep reducing the cost of this technology and raising the profits, the solar industry is constantly seeking ways to maximize the efficiencies and minimize the losses and the costs associated with the energy production process.

The PV performance is constantly affected by external environmental factors, which can lower the energy generation. One of these factors, often unmarked and underestimated, is the process known as soiling, whereby dirt, dust, and organic/inorganic contaminants deposit on the surface of a PV module. Soiling absorbs, reflects, and scatters part of the irradiance (Figure 1), reducing the intensity of the light reaching the PV cell, therefore converting into electricity (Smestad et al., 2020). The regions with high irradiances and more PV-prone are generally arid areas with also high risk of soiling. This can be due to high concentrations of particles in the air, occasional dust storms, and/or limited rainfalls (Herrmann et al., 2014; Jones et al., 2016). Unlike other PV losses, soiling is reversible, as it can be removed artificially or naturally. In addition, appropriate mitigation strategies can reduce the rate at which soiling deposits (e.g. through anti-soiling coatings or overnight inverted stowing) and, in some cases, limit its effects on the electrical PV performance (e.g. through an optimized module design) (Ilse et al., 2019b). Addressing soiling adequately makes it possible to maximize the energy performance, reduce the levelized cost of electricity (LCOE), increase the profits, and minimize the cleaning costs and the financial risks of the PV investment.

A recent analysis of soiling in the top 22 countries per PV capacity estimated that soiling caused in 2018 losses equivalent to 3%–4% of the global energy yield, with total missed revenues of at least 3 to 5 billion euros (Ilse et al., 2019b). Assuming a medium growth scenario, the same study estimated that the energy losses could raise to percentages between 4% and 7% in 2023, with up to 7 billion euros lost worldwide every year. Along with the increased PV capacity, which increases the magnitude of the economic losses even if it does not necessarily affect the fraction of energy lost, there are additional factors expected to raise the future impact of soiling. These include the increasing deployments of PV in high-insolation and high-soiling regions, and the lowering electricity price, which makes soiling mitigation less economically convenient if its cost is not reduced.

[1]Advances in Photovoltaic Technology (AdPVTech), CEACTEMA, University of Jaén (UJA), Las Lagunillas Campus, Jaén 23071, Spain

*Correspondence: lmicheli@ujaen.es

https://doi.org/10.1016/j.isci.2021.102165

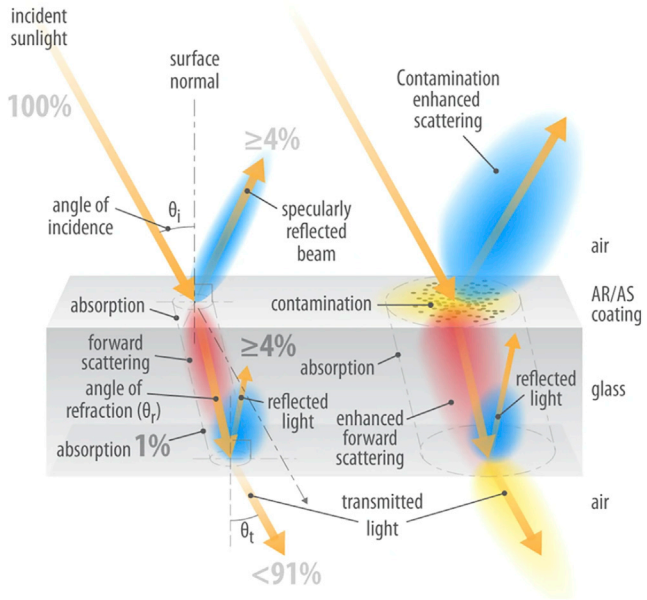

Figure 1. Sunlight absorption, reflection, and deflection due to soiling deposited on a PV glass surface
Image made by Al Hicks (NREL) and presented in (Smestad et al., 2020).

An optimized soiling mitigation strategy has multiple advantages. First, it raises the PV owners' revenues, because it increases the energy production with limited additional costs. Second, the extra energy produced raises the PV capacity factors, increasing the percentage of energy supplied by PV without considering the deployment of new PV systems. Last, the higher economic margins attract more investments and favor the installation of new PV capacity, further increasing the contribution of PV to the local, national, and global energy markets.

However, despite its global impact, soiling is a site-specific phenomenon with temporal and spatial variations and therefore has to be addressed locally (see "soiling variability and monitoring market" section for more details). Based on this principle, the soiling mitigation strategy must be planned according to the characteristics of the system (e.g. PV module design, tilt angle and orientation, tracking configuration, etc.), of the location (e.g. weather and environmental conditions, seasonality, etc.), and of soiling (e.g. dust properties) (Ilse et al., 2018; Jamil et al., 2017; Mondal et al., 2018). These intrinsic complexity and variability of soiling make the constant monitoring an essential activity to optimize soiling mitigation (Figure 2).

In addition to the variability of soiling, it should be noted that also the variability of electricity price, operational and labor costs, discount rate, and taxes can affect the profitability of soiling mitigation (Al-Housani et al., 2019; Alzubi et al., 2018; Fathi et al., 2017; Jones et al., 2016; Micheli et al, 2020d, 2021; Stridh, 2012). For these reasons, several models have already been presented to optimize the soiling mitigation strategy (i.e. maximize the difference between additional revenues and costs), depending on the environmental and economic characteristics of each site (Besson et al., 2017; Jones et al., 2016; Rodrigo et al., 2020; You et al., 2018). Despite their differences, all these models require an accurate monitoring of the losses and the understanding of their seasonality and inter-annual variability, which are discussed in this work.

Many reviews on the effects of soiling on solar technology have been presented in the past. Sarver first and, more recently, Costa and coauthors have presented comprehensive reviews on all the aspects of soiling (Costa et al, 2016, 2018; Sarver et al., 2013). They also showed the exponential growth in the number of yearly publications on soiling presented in the last decade. Figgis et al. (Figgis et al., 2017) reviewed, in 2017, the knowledge on particle deposition, rebound, and resuspension, using also experimental data collected in Qatar. Ilse et al. (Ilse et al., 2018) studied the theory behind the soiling particle deposition and removal processes, with particular focus on arid and semi-arid regions. Different authors have also reviewed the state of the art of soiling mitigation. Sayyah et al. (Sayyah et al., 2014) and Jamil et al. (Jamil et al., 2017) discussed the advantages, the disadvantages, and the potentials of the soiling mitigation

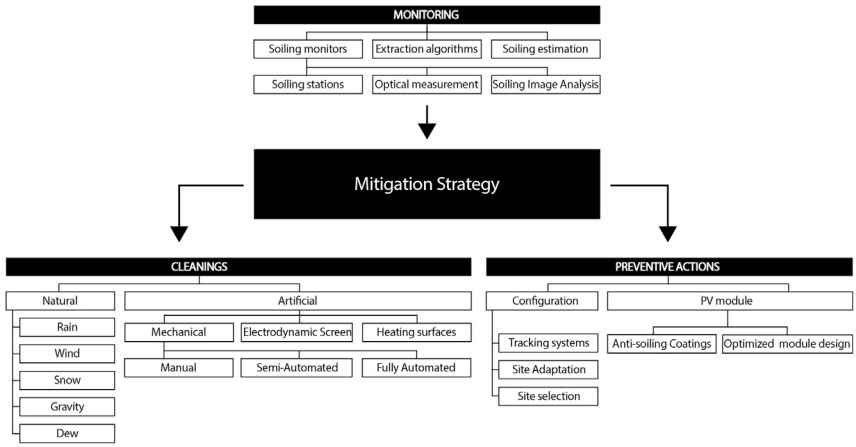

Figure 2. Description of the soiling monitoring and mitigation strategies
Partially built on previous flowcharts from (AlDowsari et al., 2014; Gupta et al., 2019; Jamil et al., 2017; Mondal et al., 2018).

techniques. The PV cleaning methods were reviewed also by Gupta et al. (Gupta et al., 2019), who described the impact of soiling on the thermal optical and electrical characteristics of PV modules as well. Ilse et al. (Ilse et al., 2019b) presented an assessment of the soiling mitigation technologies, discussing potential effects, limitations, and application scenarios and calculating their maximum allowed costs.

As mentioned, soiling monitoring is a necessary step to plan the most adequate soiling mitigation approach but has not been assessed adequately and specifically. To date, only the 2016 work from Figgis et al. (Figgis et al., 2016a) has reviewed the soiling measurement techniques, highlighting several research directions that have been explored later. Since then, the soiling monitoring market, which is also one of the topics of the present work, has expanded, with the introduction of new technologies and the identification of new potential approaches.

The aim of the present work is to sum up and discuss the current approaches, strategies, and techniques to monitor and estimate PV soiling losses. These are not limited to currently available soiling measurement techniques, as several authors have also investigated the possibility of estimating soiling indirectly from more widely available environmental parameters, such as rainfalls or pollution indexes. These methods represent powerful tools for soiling monitoring and mitigation, as they make it possible to quantify the losses even when no PV data or sensors are available, and, for this reason, are included in the review. The present study makes use also of original experimental soiling and PV data, collected in the South of Spain, to compare the various monitoring and estimation techniques. The present work can be of use for the wide PV community, because (1) it discusses the research lines where more efforts are still needed, and (2) it can help PV owners and operators identify the most appropriate PV soiling monitoring tools.

This study is structured as follows. In the "experimental setup" section , the experimental setup used to collect the outdoor soiling and PV data is described. The metrics commonly used to quantify soiling are then presented in "soiling metrics". In "soiling variability and monitoring market", the reasons behind the need for a continuous and distributed soiling monitoring are discussed, and the size of the global soiling monitoring market is estimated and forecasted. In "soiling monitoring instrumentation", the state of the art of the currently available monitoring techniques is presented, along with some upcoming and some new potential approaches. Soiling extraction algorithms are discussed in "soiling extraction algorithms". In "estimation of soiling from environmental parameters", the soiling estimation techniques, intended as methods to quantify soiling through the measurement of environmental parameters, are reviewed. Last, the state of art of soiling monitoring is summarized in "outlook", where an economic analysis is also presented.

EXPERIMENTAL SETUP

Some experimental data are used in the following sections. The data were collected in Jaén, a non-industrialized city in the south of Spain, with a population of ~110,000 inhabitants (Instituto Nacional de Estadística, 2019; Nofuentes et al., 2017) and an annual irradiation $\geq$1800 kWh/m^2 (Jiménez-Torres

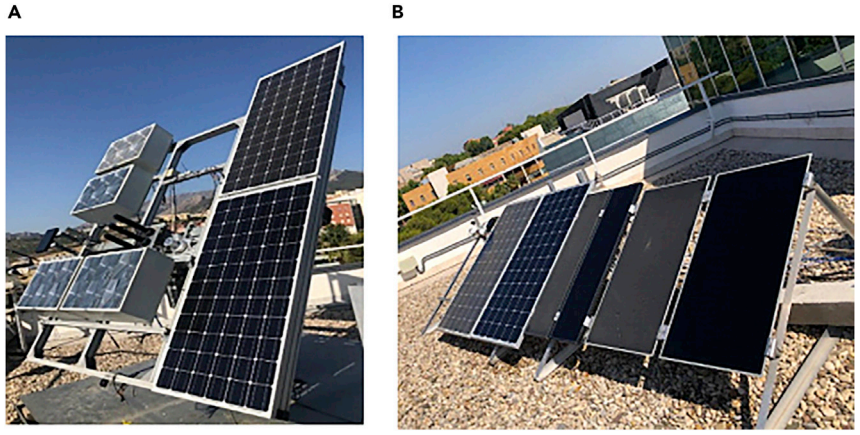

Figure 3. Experimental setup

Two-axis tracker system (A) and fixed tilt structure (B) installed on the roof of the Center for Advanced Studies on Earth, Energy and Environment (CEACTEMA), at the University of Jaén, in Jaén, Spain.

et al., 2017). As of 2019, Andalucía, the region where Jaén is located, is home to about 20% of the Spanish PV power capacity and has seen its capacity grow by more than 120% between December 2018 and July 2020 (OMIE, 2020). However, the long dry and arid summers, the occasional dust storms, and some human activities, such as harvesting or olive tree branches burnings, make the PV installations significantly affected by soiling, with power drops that can be higher than 20% (Micheli et al., 2021; Zorrilla-Casanova et al., 2012).

The PV data employed in this study are sourced from the equipment of the outdoor PV laboratory on the rooftop of the Center for Advanced Studies on Earth, Energy and Environment (CEACTEMA) of the University of Jaén. The laboratory counts a two-axis tracker and a fixed structure mounted at 30° tilt facing south (Figure 3). Two Si modules (Luxor LM-200M) and two 500x concentrator photovoltaic (CPV) modules (see (Fernández et al., 2017) for further details of the technology) are installed on the tracker. Two CIGS modules (Shell Solar ST40), two CdTe modules (First Solar FS Series 3), an Si module (Luxor LM-200M), and a commercial soiling station (i.e. soiling measurement system) are mounted on the fixed structure. One of the modules of each pair installed on the tracker and on the fixed structure is manually cleaned every week. The soiling measurement system, provided by Atonometrics, is made of a reference PV cell automatically cleaned every morning through a high-pressure DI water jet. Soiling is quantified by comparing the output of the reference cell and that of the Si module mounted nearby, following the procedure described in "soiling metrics". The IV curves and the temperatures of both the dirty and the clean modules are recorded at a 5-min interval.

The daily soiling data shown in this work have been recorded between March 2019 and May 2020. The soiling station produces two soiling loss time series: one based on the short-circuit current and one based on the maximum power data. The differences between the two measurements are described in "soiling metrics". At this stage, it is important to highlight that the experimental soiling losses employed in this work are calculated using the short-circuit current.

The rainfall data have been measured by a weather station, MTD 3000C from GEONICA, installed on the same terrace. This station also records direct normal irradiance, wind speed, relative humidity, and air temperature. Daily rain data have been obtained as sum of the rain accumulated on each day. In addition, also the particulate matter data, intended as concentration of solid and liquid particles suspended in the air, have been collected. The particulate matter is generally quantified through the PM_{10} and $PM_{2.5}$, indexes expressing the density of particles of diameters respectively smaller than 10 or 2.5 microns suspended in a 1 m^3 of air. The Junta de Andalucía makes available the PM_{10} concentration values recorded at 10-min intervals by a monitor located in "Ronda del Valle," less than 1 km from the University of Jaén (Consejería de Medio Ambiente, 2020). In this work, these PM_{10} data, available until the end of May 2020, have been averaged into daily values.

The soiling loss profile recorded during the data collection period is shown in Figure 4, expressed as daily soiling ratio (see "soiling metrics" for definition), correspondent to 1-Daily Soiling Loss. A two sigma filter

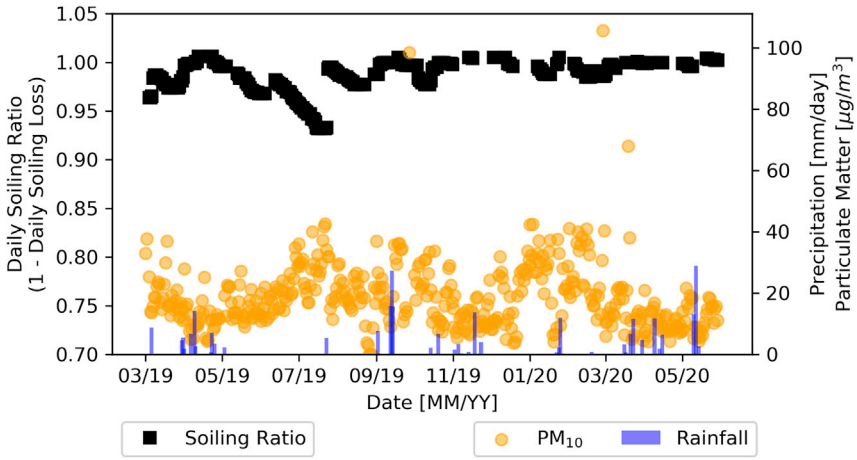

Figure 4. Soiling ratio profile (left y axis) and daily rainfall and PM_{10} patterns (right y axis)
The definition of soiling ratio (which corresponds to 1-soiling losses) is given in "soiling metrics".

has been used to remove outliers (Theristis et al., 2020). Soiling in Jaén is particularly significant in summer (loss up to 7%), generally arid and characterized by long dry periods. Two natural cleaning events were registered, a partial one in June and a full recovery in the middle of July. Although this latter is due to a rain event, the first one is probably due to high wind speed and relative humidity conditions registered in the days it occurred. The missing soiling data are due to the filtering, which eliminates cloudy days (irradiance values <500 W/m^2), and to some unexpected shading occurred in December.

SOILING METRICS

One of the most common metric used to quantify the amount of soiling deposited on PV is the *Soiling Ratio* (r_s). The latest version of the IEC 61724-1 (International Electrotechnical Commission, 2017) defines the r_s as the ratio of the actual electrical output of a PV array under given soiling conditions to the output expected if the PV array was clean and free of soiling. It is expressed as follows:

$$r_s = \frac{Z_{soil}}{Z_{clean}} \quad \text{(Equation 1)}$$

where Z is the electrical output. The "soil" subscript marks the electrical output in actual conditions of soiling, measured from an outdoor mounted sensor or directly from monitored PV modules. The "clean" subscript marks the electrical output in clean conditions, measured from a clean reference device or estimated through standard PV performance models (King et al., 2004). The electrical outputs should be measured at and/or estimated for the same time and the same conditions and should also be corrected according to the recorded irradiance and temperature values. The soiling loss, called "Soiling Level" in the IEC standards (International Electrotechnical Commission, 2017), can be calculated as 1-r_s.

The soiling ratio has a value of 1 in absence of soiling (0% soiling loss) and decreases while soiling deposits on the PV modules. A soiling ratio of 0 occurs if soiling blocks all the sunlight from reaching the cell (100% soiling loss). Indexes similar to the soiling ratio, such as the Cleanness Index (Guo et al., 2015; Javed et al., 2017a), the Soiling Loss Factor (Tamizhmani et al., 2016), and the Soiling Factor (Rodrigo et al., 2020), can also be found in literature. All these indexes are based on the same concept as the r_s: the ratio of the electrical output of a PV device to the output of the same device in clean conditions. So the higher their values (up to a maximum of 1), the lower the soiling losses.

It should be noted that, generally, the term "soiling ratio" has been used quite loosely to indicate either an instantaneous, an hourly, a daily, or an annualized value. In this work, if not specified, the term "soiling ratio" refers to the hourly value. In some studies, the average soiling ratio is obtained as an irradiance-weighted average, whereas, in this work, the average soiling ratio has been calculated as simple arithmetic mean of the daily soiling ratios.

Figure 5. Examples of non-uniform soiling, as classified by Kazmerski et al. (2018)
(A) Edge build-up, (B) waves, (C) blotch due to bird dropping. Left picture courtesy of Jesús Montes-Romero, University of Jaén (Spain). Center and right pictures by João Gabriel Bessa.

One important aspect to take into account is that the value of the instantaneous soiling losses might change depending on the electrical parameter Z used in Equation (1), which can be either the short-circuit current, I_{sc}, or the maximum power, P_{max}. The difference is due to the potential non-uniform distribution of soiling on the modules' surface. Indeed, in real conditions, soiling can accumulate on the surface with different patterns (Figure 5), classified by Kazmerski et al. 2018 as follows:

a) Edge build-up: accumulation at the edges of the modules

b) Waves: undulations caused by the wind or rain

c) Blotches: depositions of irregular shapes, including animal droppings or growth of organic contaminants

In conditions of non-uniform distribution of soiling, the cells of the module are under different shadings. These can lead to dissimilar effects on the electrical output of each cell across the module surface. Power losses up to 10% higher than the short-circuit current losses have been reported in literature in conditions of non-uniform soiling (Gostein et al., 2013). Uneven losses for current and power were also reported for a 2 MW system in Southern Spain by Lorenzo et al. (Lorenzo et al., 2014). The authors of that work highlighted the risk of hot spots associated with non-uniform soiling, which can potentially damage the cells permanently. They found that the hot spots led to temperature differences >20° between soiled and unsoiled cells. In 2015, Gostein et al. (Gostein et al., 2015) reported that soiling deposited on the bottom right corner of a PV module and covering the 0.5% of its surface caused a 9% power loss.

An example of the effects of non-uniform soiling is shown in Figure 6, where the I-V and P-V curves of the two Si modules installed on the roof of the University of Jaén ("experimental setup") in conditions of uniform (Figure 6A) and non-uniform soiling (Figure 6B) are reported. As it can be seen, under uniform conditions (Figure 6A) the soiled and clean I-V and P-V curves have the same shape, and soiling produces a similar reduction in the maximum power and short-circuit current compared with the clean curve. As a consequence, the soiling ratios estimated using the two parameters are similar (r_{sIsc}=0.99, r_{sPmax} = 0.97). However, under non-uniform soiling (Figure 6B), the soiled I-V and P-V curves present a step in the region of the maximum power. This is due to the fact that shaded cells are bypassed by the diodes, reducing the power output, but not affecting as much the short-circuit current. As a consequence of the non-uniformity shown in Figure 6B, the soiling ratios estimated using the short circuit current and the maximum power are markedly different (r_{sIsc}=0.97, r_{sPmax} = 0.65). The effects of non-uniform soiling are similar to those caused by partial shadings (Schill et al., 2015) and, in extreme cases, can lead to even more than one knee in the I-V and the P-V curves (Figure 6C).

The impact of the non-uniform soiling distribution on the whole PV module's performance changes depending on the modules' architecture and, in particular, on the bypass diodes' configuration. Because of this, solutions to mitigate the effects of non-uniform soiling can already be put in place. For example, the orientation of the PV module can force the deposition of non-uniform soiling over multiple strings rather than on a single one (Gostein et al., 2013), potentially preventing the bypass of a full string. In addition, the use of half-cell or frameless modules or of different configurations

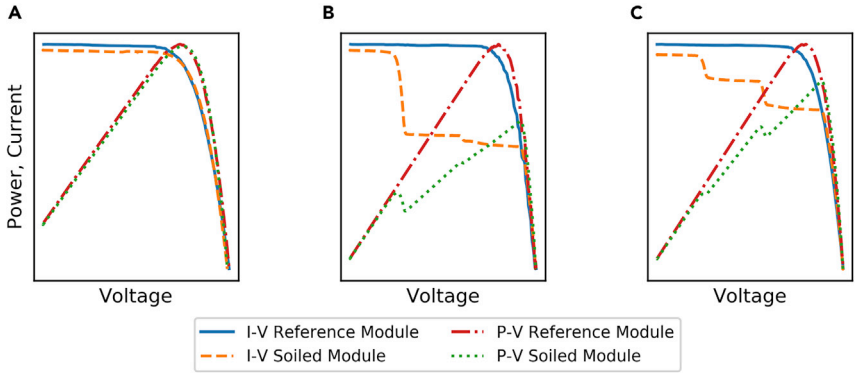

Figure 6. I-V and P-V curves for uniform and non-uniform soiling conditions

I-V and P-V curves for days with soiling uniform (A), non-uniform (B), and partial shading (C) for a Si module installed in Southern Spain.

of cell strings and bypass diodes can lower the risk of non-uniform soiling deposition or, at least, minimize its effects (Ilse et al., 2019b).

As mentioned, the parameter Z used in Equation (1), whether current or power, has to be corrected to prevent non-soiling-related issues, such as the temperature, from biasing the soiling quantification. It is important to highlight that the soiling ratio varies also with the time of the day, depending on the angle of incidence (Burton et al., 2016), with generally higher values (i.e. lower losses) in the middle of the day (Figure 7). Zorrilla-Casanova et al. (Zorrilla-Casanova et al., 2012) analyzed this behavior and found that it is the result of the variation of the direct radiation (whose percentage loss increases with the angle of incidence) and of the diffuse radiation (whose percentage loss is independent of the angle of incidence) during the different hours of the day. Mainly for this reason, the IEC 61724-1 standards (International Electrotechnical Commission, 2017) recommend calculating the soiling ratio using only data measured within ± 2 h of solar noon for fixed tilt systems or for angles of incidence under 35° for active tracking systems. This way, the losses are calculated only for the hours of highest irradiance and energy production. In addition, this approach allows also to minimize the effects of angular misalignments (Gostein et al., 2014) and potential morning and evening shadings (Micheli et al., 2016). Other authors (Figgis et al., 2016a) have instead suggested to use time-integrated soiling measurements, rather than instantaneous, to characterize the effective impact of soiling on the energy yield.

A second commonly used parameter is the *Soiling Rate*, which describes the daily rate at which the soiling ratio decreases while soiling deposits on the PV surfaces. It is a measure of the slope of the soiling ratio profile for a specific period and is expressed in %/day. Because the soiling ratio decreases while soiling accumulates, the soiling rate is conventionally reported with negative values. At least two different methodologies have been proposed to calculate the soiling rate from a daily soiling ratio profile:

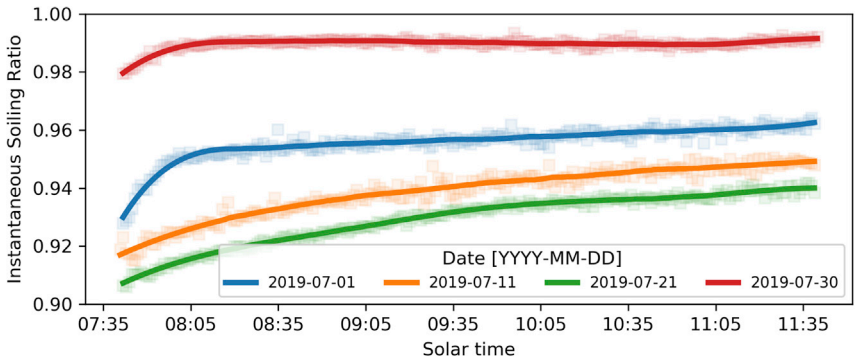

Figure 7. Variation of instantaneous soiling ratio values in some summer mornings in Jaén, Spain

For better readiness, each curve, colored depending on the day, has been obtained by smoothing the measured data (squared markers) through a Savitzky-Golay filter (polynomial of third order with 71 coefficients).

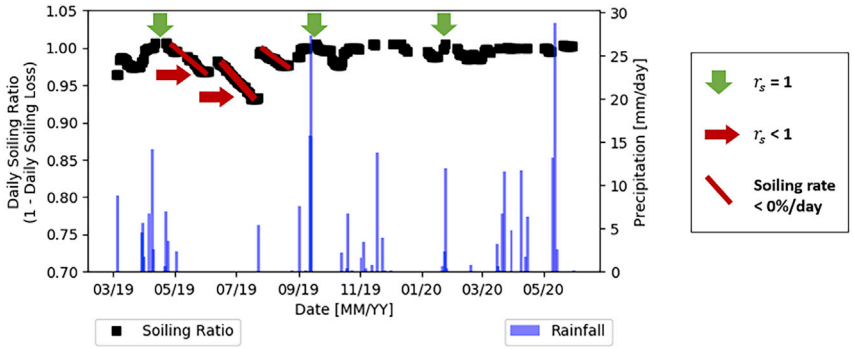

Figure 8. Examples of soiling ratios and soiling rates for the soiling measured in Jaén

Green arrows indicate some days with 0% losses ($r_s = 1$). Red arrows indicate the period where the r_s value decreases. The negative slopes (soiling rates) in these periods are also highlighted.

i. Fit of the soiling ratio profile during the longest period without artificial or natural cleanings, calculated by using the least-square regression (Kimber et al., 2007).

ii. Median of the best fits of any period of at least 14 days without artificial or natural cleanings calculated by using the Theil-Sen estimator (Deceglie et al., 2018b).

The Theil-Sen estimator returns the median of the slopes of all the lines connecting each pair of data points within a dry period. It was recommended by Deceglie et al. (Deceglie et al., 2018b) because more robust to outliers and unaccounted cleaning events. To address the same issue, Besson et al. (Besson et al., 2017) used, instead, a weighted least-squares approach.

Figure 8 presents a summary of the soiling metrics described previously, based on the measurements detailed in "experimental setup" and shown in Figure 4. Green arrows mark some of the dates in which the soiling ratio is equal to 1 (i.e. 0% soiling losses). The soiling ratio value decreases during the dry periods indicated by red arrows. The soiling rates (slopes of the descending soiling ratio profiles) in some of these periods are also highlighted.

SOILING VARIABILITY AND MONITORING MARKET

Soiling is the result of the interaction of a number of factors related to the environment and the climate of the location, the configuration of the system, and the design of the modules. For these reasons, it can change from location to location and with time. In some cases, different soiling losses can be experienced by different strings and modules even within the same plant.

A uniform soiling distribution (i.e. all the PV modules in a plant soil at the same rate and experience the same losses) is a common assumption made in most of the researches addressing soiling. However, the spatial variability of soiling deposition is an important issue, as it can make economically worth cleaning only some of the strings rather than the full PV system (Ilse et al., 2019b). This non-uniformity occurring at system level should not be confused with the module-level non-uniformity discussed in "soiling metrics".

In addition, the rate at which soiling deposits and the frequency of natural cleanings can change with the seasons and can also vary from year to year, following the variability of weather and environmental conditions. In their soiling mechanisms review, Ilse and coauthors (Ilse et al., 2018) mapped the temporal and spatial variability of the various parameters related to soiling (Figure 9). Understanding the variability of soiling, and potentially its non-uniform distribution, can be beneficial, if not essential, to put in place an optimal mitigation strategy. The current knowledge on soiling non-uniformity and temporal variablility is reviewed in the next subsections.

Spatial non-uniformity

A number of studies have reported cases of different soiling deposition for two or more nearby sites. In 2011, Massi Pavan et al. (Massi Pavan et al., 2011) found a significant difference in the soiling losses

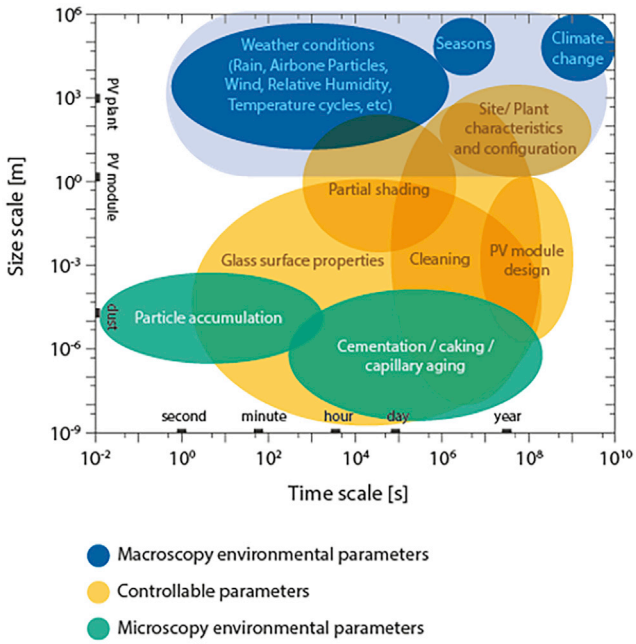

Figure 9. Time and size scales of factors affecting soiling, adapted from (Ilse et al., 2018)

experienced by two 1 MW PV systems installed in the same region in Italy and that visually seem within 60–70 km of each other. According to the authors, the difference was mainly due to the fact that one site was built on sandy ground (power losses up to 6.9%), whereas the other on a more compacted ground (power losses up to 1.1%). Two years later, Mejia and Kleissl (Mejia and Kleissl, 2013) analyzed the soiling losses of 186 PV sites in California and found a factor of 3x between the average soiling rate of 75 Southern California Edison sites and that of 35 sites of the San Diego Gas and Electric. Cordero et al. (Cordero et al., 2018) showed how soiling changes through a 1300-km long transect in the Atacama Desert, with average soiling rates ranging from <0.05%/day to >0.4%/day. Despite these findings, an investigation conducted using the 83 soiling data points of the NREL soiling map (National Renewable Energy Laboratory, 2018a) showed that, through the use of spatial interpolation techniques, it can still be possible to estimate the average losses at a location knowing the soiling losses of nearby sites (Micheli et al., 2019a). However, the best results were obtained if the nearby sites were within 50 km and if these had similar features to the investigated site (e.g. all fixed or ground-mounted PV systems or all locations in "non-developed" areas).

As mentioned, spatial non-uniformity can affect the soiling deposition at system-level as well. Gostein et al. (Gostein et al., 2014) showed differences in losses up to 3% among the strings of a PV system during a short soiling intense period. In following investigations, Gostein et al. (Gostein et al., 2018b) analyzed the soiling rates measured by soiling stations distributed across two Californian PV sites. The authors found that the average soiling rates could vary by up to 2x within the same site (Figure 10). Interestingly, the higher deposition rates in the site shown in Figure 10 were measured by those soiling stations located closer to a nearby farm, along the average wind direction. All these studies confirm the necessity of measuring the soiling losses at multiple locations within the same PV system and open to the possibility of performing cleaning only on determined strings, if economically viable.

Temporal variability

Soiling can significantly change with time. High- and low-soiling periods can alternate over the course of months and seasons. These can be due to the seasonal variation of environmental factors causing soiling, to periodic human activities (such as harvesting) or to exceptional events, such as dust storms or construction works. Even sites with low average losses can benefit substantially of soiling mitigation, if, for example, cleanings are performed in the highest soiling seasons (Micheli et al., 2021). Several works have highlighted the more pronounced soiling losses occurring during summer in California (Caron and Littmann, 2013; Kimber et al., 2007;

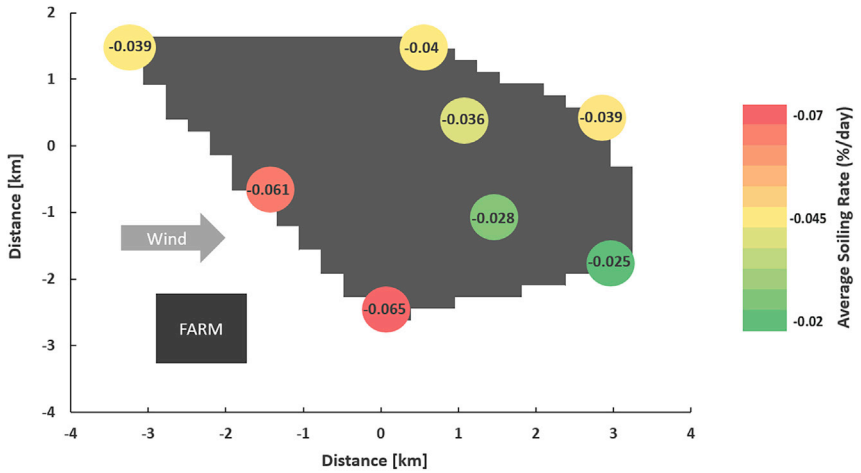

Figure 10. Within-site variability of average soiling rate in two different locations in California, USA, adapted from (Gostein et al., 2018b)

Mejia et al., 2014; Mejia and Kleissl, 2013). On the other hand, various authors have reported higher soiling rates in winter than in summer in Santiago, Chile (Besson et al., 2017; Cordero et al., 2018) and in Doha, Qatar (Javed et al., 2020), as a result of the specific particle matter concentration pattern. Other examples of seasonal soiling have been reported in the South of Spain (Micheli et al., 2021; Zorrilla-Casanova et al., 2012), where most of the losses typically occur during the long dry summer. A metric, named Soiling Variability Index, was proposed to quantify the seasonality of soiling (Micheli et al., 2017b). This index, based on a similar parameter used to describe the degree of variability of rainfalls (Walsh and Lawler, 1981), can be used to classify soiling depending on the number of months in which most of the losses are experienced.

In most cases, seasonal soiling is due to prolonged seasonal dry periods (Conceição et al., 2020), but this is not the only reason. Indeed, the temporal variability of soiling can be also the result of other natural or man-driven phenomena. Caron and Littman (Caron and Littmann, 2013) identified seasonal tilling and harvesting activities as temporary seasonal soiling emitters. Also the concentration of pollen, for example, follows strongly seasonal patterns (Conceição et al., 2018a).

As mentioned, even extraordinary events, which do not recur at regular intervals, can temporarily affect the soiling accumulation and make soiling monitoring essential. For example, construction activities can cause unexpected significant soiling losses (Schill et al, 2011, 2015). Dust storms or dust-laden winds can cause sudden drops in PV performance or increase in soiling deposition rates and periodically affect several countries worldwide, including Iraq (Kazem et al., 2014), Saudi Arabia (Yilbas et al., 2015), UAE (El-Nashar, 2003), India (Nahar and Gupta, 1990), Qatar (Javed et al, 2017b, 2020), and Morocco (Conceição et al., 2019a). Saharan dusts events were found to affect also the performance of PV modules in Europe, with power drops >30% in Cyprus (Kalogirou et al., 2013) and 8% in Portugal (Conceição et al., 2018b).

Significant seasonal changes in soiling deposition rates were also reported in Chile, with variations within the same site of 2x or 3x (Cordero et al., 2018). In this case, the increase in soiling loss was considered a consequence of a number of factors: a raise in relative humidity, which caused an increase in particle size and, therefore, in deposition rate; a decrease in wind speed (at least for locations with high soiling deposition); and an increase in particle concentration.

Although some of the phenomena causing seasonal soiling are sporadic and stochastic, in many cases these are recurrent and might be predicted to allow for a better soiling mitigation planning. In this light, the possibility of using weather generation algorithms to identify typical high and low rainfall (and therefore low and high soiling) periods has been investigated (Micheli et al., 2020a). Despite that, inter-annual variations in environmental and weather conditions can affect the seasonality and the year-to-year repeatability of soiling (Deceglie et al., 2017). This, in addition to the random nature

Table 1. Number of soiling sensors recommended according to the power capacity of five countries in 2017/2019 and number of sensors that would be necessary by 2024

Country	Number of sensors currently required	Sensors density [No./GW]	Capacity added by 2024 [GW]	Number of additional soiling sensors necessary by 2024
Germany	400	9	28.91	260
India	526	20	69.85	1,397
Italy	1,311	350	11.30	3,955
Spain	559	188	17.09	3,213
USA	4,376	128	102.75	13,152

The sensors density represents the average number of sensors per GW of installed capacity and is calculated according to the requirements of the standard (International Electrotechnical Commission, 2017).

of some of the seasonal soiling causes, strengthens the need for an accurate and continuous soiling monitoring.

Market size

The main objective of PV monitoring is to provide a real-time diagnostic of the energy production and to identify possible faults and energy losses, in order to maximize the energy yield, minimize the O&M costs, and avoid safety hazards (Madeti and Singh, 2017). Soiling is one of the most relevant environmental factors, along with irradiance and temperature, that can significantly affect the performance of PV systems (Gostein et al., 2014; Sarver et al., 2013). In this section, an estimate of the number of soiling sensors currently needed and required in the near future is presented.

The IEC 61724-1 standard (International Electrotechnical Commission, 2017) recommends, for high accuracy, the installation of soiling monitors at any site with expected yearly losses greater than 2%. Because of the aforementioned non-uniform deposition, more than one sensor is recommended for systems larger than 5 MW. In particular, the number of soiling sensors, which shall be the same as the number of irradiance sensors and weather stations, ranges between 1 and 8 and depends only on the size of the system.

From the list of PV systems installed in a country, it is possible to get an estimate of the number of soiling sensors currently needed. In this work, the lists of operating PV systems located in five representative PV markets were collected:

- Germany: existing power plants with a minimum net nominal capacity of 10 MW in 2017, inclusive of plants in Austria, Luxembourg, and Switzerland that feed into German grid. It includes also 22 power plants <10 MW and eligible for payment according to the Renewable Energy Sources Act (Federal Ministry for Economic Affairs and Energy, 2017). Sourced from the German Federal Network Agency (Bundesnetzagentur, 2017).
- India: installed capacity in India with net nominal capacities ranging from 1 MW to 1500 MW in 2019. Sourced from the Ministry of New and Renewable energy of India (Government of India, 2019).
- Italy: existing power plants with minimum net nominal capacity of 1 MW up to October 2019. Sourced from (Energy Services Manager GSE SpA, 2019).
- Spain: existing power plants with minimum net nominal capacity of 1 MW up to October 2019. Sourced from the Spanish Ministry for the Ecological Transition (Electra Spain, 2019).
- USA: existing power plants with minimum net nominal capacity of 1 MW up to July 2019. Sourced from the U.S. Energy Information Administration (U.S. Energy Information Administration, 2019).

The analysis was conducted by assuming expected soiling losses higher than 2% in each site (i.e. soiling monitoring recommended for all the sites and high accuracy according to the standards). As shown in Table 1, the average number of sensors per unit of installed capacity (here called "Sensors density" and expressed in number of sensors per GW) strongly varies from country to country, depending on the

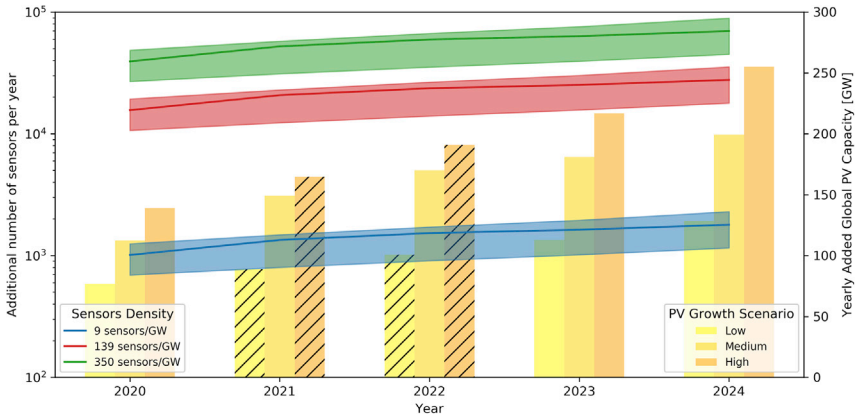

Figure 11. Soiling sensors' market analysis based on different scenarios of PV capacity growth and sensor density

The three lines show the number of sensors needed per year. The bars represent the additional PV capacity installed per year as forecasted by (Solar Power Europe, 2020). Missing PV capacities have been determined through linear regression and are marked with hatches.

distribution of PV systems' sizes. Because of the non-linear relationship between system size and number of sensors recommended by the standards, countries that have the capacity distributed in smaller systems have a larger sensor density. On the other hand, the larger the average PV system in size, the lower the sensors density. For example, the high number of sensors/GW in Italy is due to the fact that 85% of the power plants in the Italian database are in the range 1 MW–5 MW. For India, only 58% of the listed power plants are in this range. In addition, it should be noted that Germany's low sensor density is probably also the result of the fact that only few systems <10 MW are reported, representing 14% of the total capacity.

According to the results, shown in Table 1, more than 7,000 sensors are already required in these five markets, which altogether represented the 32% of the 2019 worldwide PV capacity (Solar Power Europe, 2019). By assuming that the country-specific sensors densities will not change, the study can be extended to predict the number of sensors that will be required in future. By using the medium PV capacity growth scenario reported in (Solar Power Europe, 2020), it is found that, until 2024, a total of almost 22,000 sensors will be needed just to cover the newly installed capacity for the five considered countries (Table 1).

This same analysis can be repeated for the global PV capacity, by assuming three representative sensors' density scenarios: low density (9 sensors/GW, as of Germany), high density (350 sensors/GW, as of Italy), and intermediate density (139 sensors/GW, obtained as average of the five countries). The Global Outlook 2020–2024 (Solar Power Europe, 2019) presents three potential PV capacity growth scenarios: low, medium, and high. The results of the analysis for the three density scenarios and the three PV growth scenarios are reported in Figure 11. Considering an intermediate sensors density, it is found that almost 60,000 sensors are already needed to cover the rest of the global capacity outside of the five countries of Table 1 (not shown). Additional 15,000 sensors will be required to cover only the new global capacity installed in 2020. These will become more than 25,000 in 2024, just to cover the newly added capacity in that year.

The present analysis is based on different assumptions. First, the density of sensors is maintained constant throughout the years. Second, all the sites are assumed to install soiling monitors and in a number equal to that recommended by the standards for the highest accuracy. The results are also based on the best PV system size information that was available at the time of the study. It is acknowledged that this information might be incomplete and could lead to different results in the future. Nevertheless, these numbers give an idea of the size of the soling sensor market and explain the reason behind the several monitoring solutions currently available and assessed in the following sections.

SOILING MONITORING INSTRUMENTATION

In this section, the techniques being used nowadays for soiling monitoring are assessed and their features and limitations are discussed. The most accurate method to quantify soiling is through the measurement of

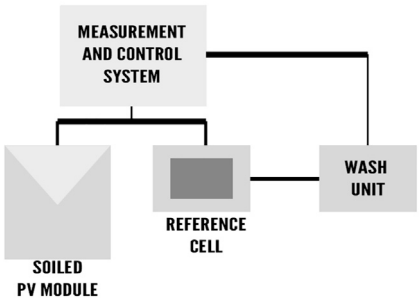

Figure 12. Diagram of a typical structure of an automatically cleaned soiled station

an I-V curve, as it directly provides information on the intensity of the losses and the presence of non-uniform soiling deposition (Schill et al., 2015). However, the continuous or at least regular measurement of multiple modules can be unrealistic, expensive, and exposed to large errors if the irradiance sensors are not clean (Shrestha and Taylor, 2016). For these reasons, different continuous and automatic solutions have been proposed for soiling monitoring, with the aim of reducing at minimum the requirement for human labor and the cost. Nowadays, at least three different product categories are available to monitor the soiling of fielded PV systems: soiling stations, optical soiling measurement (OSM) sensors, and soiling image analysis (SIA) sensors. The first class of sensors directly measures the effect that soiling has on the electrical losses of PV. The second class, instead, estimates the losses by measuring the optical properties of soiling. The third one aims to quantify the surface of PV modules covered by soiling through aerial image analysis methods.

Soiling stations

Currently, soiling stations are the most common commercially available solutions to monitor soiling. They consist of at least two PV devices, one of which is left to soil naturally, whereas the other one is cleaned manually or automatically at regular intervals (Gostein et al, 2014, 2015). The electrical outputs of the two devices are compared to calculate the soiling ratio, according to the methodology described in "soiling metrics". In Figure 12, the diagram of an automatically washed soiling station, made of a reference cell, a PV module, and a water-based wash unit is shown. This is not the only configuration available, as, for example, in some cases, cleanings can be done manually, without the need of a washing unit, and/or the reference cell can be replaced with a full-sized module (and vice versa). In some cases, cleanings can be performed mechanically and without the need of water, for example through the action of a rotating brush (Toth et al., 2020).

Despite being a simple solution to measure soiling of PV systems, soiling stations do not eliminate the need for regular cleanings and maintenance, which can be expensive, especially in remote locations. On the other hand, also automatic soiling stations present some disadvantages due to potential imperfect cleanings in severe soiling conditions and partial non-uniform cleanings that can leave the edges and the corners of the reference device soiled. In addition, the water tanks need to be refilled regularly, whereas mechanical parts, such as rotating brushes, might have reliability issues. Incorrect or undone cleanings can result in a significant measurement uncertainty (Muller et al., 2018a).

In order to overtake some of these drawbacks, a waterless single-cell soiling station has been proposed by a team of the Arizona State University (Curtis et al., 2018). This consists of a single solar cell that is covered by a PV glass, where soiling deposits. The cell operates both as soiled and reference sensor: the clean measurement is taken thanks to an automated system that removes the glass from the top of the cell.

Optical soiling measurement

In an effort to lower the cost and increase the reliability of soiling monitoring, a new class of soiling monitors has been developed, and some sensors have been already launched in the market. Optical soiling measurement (OSM) sensors estimate the soiling ratio from the optical characteristic of the soiling accumulated on a PV glass. Typically, they are designed to need no water or cleanings, to require no or limited

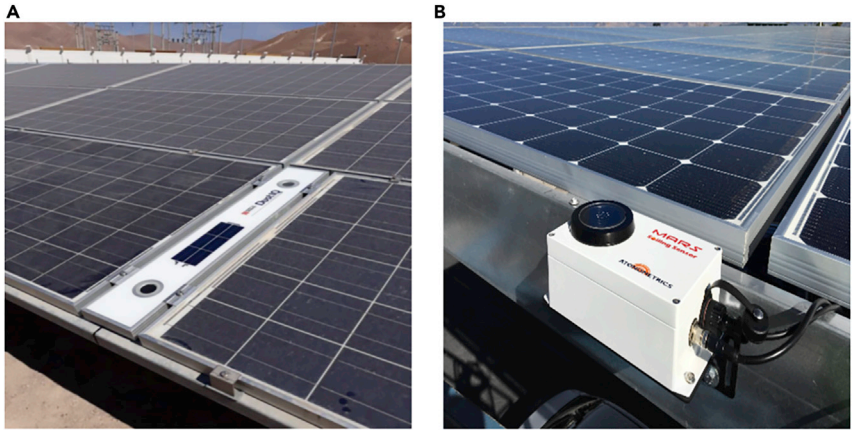

Figure 13. Commercial OSM detectors

(A) DustIQ installed in Morocco, courtesy of Mark Korevaar (Korevaar et al., 2018).

(B) Mars Soiling Sensor, courtesy of Bill Stueve (Gostein et al., 2019).

maintenance, and to have no moving parts. Kipp&Zonen's DustIQ (Korevaar et al., 2017) and Atonometrics' Mars Soiling Sensor (Gostein et al., 2018a) have been the first two commercial OSM devices. In the DustIQ detector (Figure 13A), a monochromatic light is emitted on the back of a soiled glass, and the reflection is measured with a photodiode and used to estimate the soiling losses. The Mars Soiling Sensor (Figure 13B) measures the impact of soiling on the brightness of the image taken by a digital camera. These two new systems are currently being field tested, and the preliminary results show good correlations between their optical measurements and the measurements of the traditional soiling stations (Gostein et al., 2019; Korevaar et al., 2019). A first field comparison of three soiling stations and the two aforementioned OSM sensors is being conducted by GroundWork Renewables, Inc. (Morley et al., 2020) in Logan, Utah, USA. The results of the first year of investigation (May 2019–May 2020) showed that all the sensors were able to distinguish high- and low-soiling periods, with up to 2% errors in monthly soiling rate estimations from OSM detectors compared with 1% errors from soiling stations.

Image processing techniques have been applied in different OSM solutions. First, they were used by Figgis et al. (Figgis et al., 2016b) to measure the soiling deposition and resuspension rates. A portable digital microscope, designed to face the back surface of a glass coupon where soiling accumulated, was used to take pictures of the deposited particles. The authors used a code implemented in the image processing software package *ImageJ* to calculate the surface coverage, which was then used to estimate the mass of the deposited dust and the transmittance loss. The microscope in Figgis et al. (2016b) was successfully used to measure the deposition and the resuspension of any particle larger than 10 μm^2 in Doha, Qatar. A similar set up was recently employed in a field study in Gandhinagar, Gujarat, India (Valerino et al., 2020). After an initial calibration, the microscope was found to return soiling loss estimations within 1% of the losses measured with a commercial soiling station.

Several authors have reported linear correlations between surface coverage and transmittance losses (Bahattab et al., 2016; Burton et al., 2016; Einhorn et al., 2019; Figgis et al., 2016b; Micheli et al., 2017a; Naumann et al., 2018; Smestad et al., 2020), which are summarized in Figure 14. The slope of the linear correlation is not the same in the different studies, even because it can be affected, for example, by the wavelength range considered for the transmittance measurements (Micheli et al., 2020b). Despite that, given the high quality of each study's correlation, there might be the possibility to tune each specific area-coverage measuring device to minimize the error in the estimation of the transmittance.

A different OSM detector, named "DUSST," estimates the soiling ratio by measuring the transmittance of a monochromatic light emitted by a known collimated source and transmitted through a naturally soiled glass (Muller et al., 2018b; Solas et al., 2020). Compared with the other OSM sensors, DUSST directly measures the loss in the transmitted component of the light, which is the one responsible for the electrical loss. A one-year experimental study conducted in Spain demonstrated that soiling losses of various PV

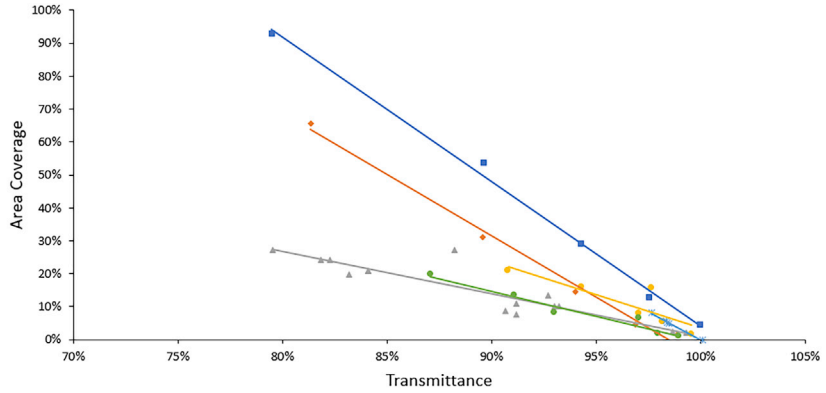

	Figgis et al.	Burton et al.	Smestad et al.	Naumann et al.	Bahattab et al.	Einhorn et al.
Slope	-3.72	-1.28	-2.01	-3.72	-1.5	-3.33
τ(λ) range (μm)	0.30-3.00	N.A.	0.35-1.10	0.32-1.30	0.38-0.78	0.30-1.25

Figure 14. Experimental area coverage data versus relative transmittance values reported in (Bahattab et al., 2016; Burton et al., 2016; Einhorn et al., 2019; Figgis et al., 2016a, 2016b; Naumann et al., 2018; Smestad et al., 2020)

All transmittance values have been converted into relative values.

technologies could be estimated with good accuracy by using only monochromatic transmittance measurements at selected wavelengths in the 0.5 μm–0.6 μm range (Micheli et al., 2019c). In particular, it was found that each PV material had a preferred wavelength at which the measurement returned the lowest estimation error. A recent indoor characterization showed that DUSST could measure soiling losses with errors <1.4% (Solas et al., 2020).

All the OSM sensors presented so far make use of a single optical measurement to estimate the soiling losses. Therefore, they assume a flat transmittance profile across the light spectrum. However, the transmittance spectrum of soiling is lower in the blue region, i.e. shorter wavelengths, and gradually increases with the wavelength. This means that a single wavelength value can differ substantially from the average value of the full spectrum (Figure 15A). In addition, each PV material has a specific spectral response, converting photons of different energies at different efficiencies. This means that the same soiling profile can have dissimilar effects on different PV materials (John et al., 2016; Qasem et al., 2014). This effect can be worsened or counter-balanced by the spectral distribution of the irradiance itself, which varies every instant depending on the location, the solar position, and the atmospheric conditions.

As mentioned, single wavelength transmittance measurements can be successfully used to rank the severity of soiling and to differentiate between high and low soiling conditions (Micheli et al., 2019c). Despite that, the actual soiling loss calculation can be subjected to a bias because of the non-flat shape of the soiling spectral transmittance. A recent study (Smestad et al., 2020), based on the analysis of soiling collected at seven locations in five countries, proposed the use of the following modified version of the Ångström equation (Ångström, 1929) to model the spectral distribution of soiling transmittance, independently of the soiling composition or of the location (Figure 15B):

$$\tau(\lambda) = \exp\left(-\beta^*_{sur} \cdot \lambda^{-\alpha^*}\right) + \gamma^* \qquad \text{(Equation 2)}$$

where $\tau(\lambda)$ is the spectral transmittance at a wavelength λ and α^*, β^*_{sur}, and γ^* are wavelength-independent variables. This equation can be solved (i.e. the values of the three variables can be identified) in two ways: either by correlating the variables to the particle properties or by knowing the soiling transmittance values at three wavelengths. Smestad et al. (Smestad et al., 2020) showed correlations among β^*_{sur}, γ^*, and the broadband relative hemispherical transmittance and between this last and the fractional area coverage. No physical meaning was instead found for α^*, which is expected to be related to the particle size. Based on this equation, a different investigation (Micheli et al., 2020b) focused on the possibility of using a small discrete number of measurements to model the full soiling transmittance spectra. The results showed that soiling losses of different PV technologies under different irradiance conditions can be estimated with only two or three single wavelength transmittance measurements. This makes it possible to correct the soiling

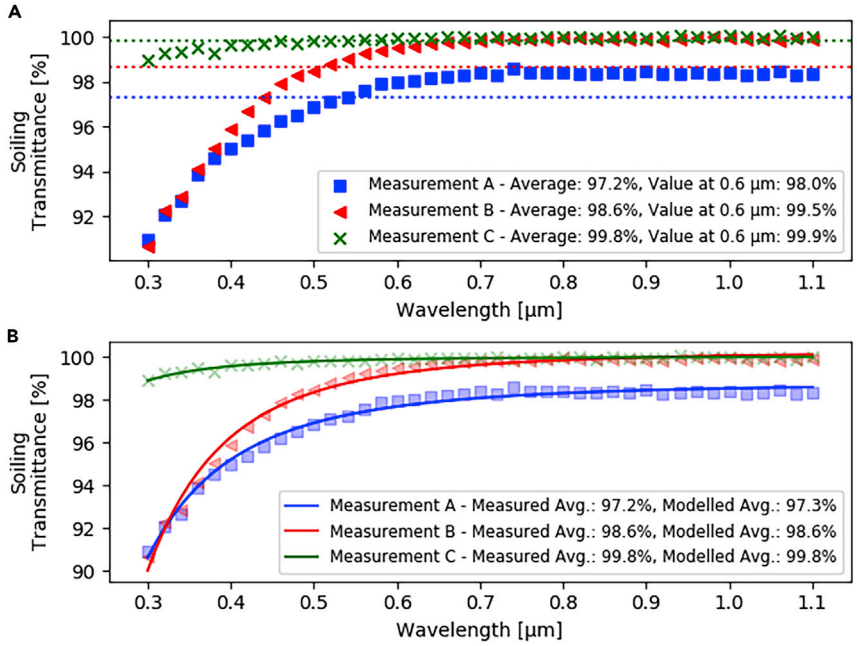

Figure 15. Relative hemispherical transmittance spectra of soiling collected on a soiled glass coupon and measured on three different days in Jaén, Spain

In (A), the difference between the mean values (horizontal dotted lines) and the value at 0.6 µm. In (B), the fits obtained by using Equation (2). Adapted from Micheli et al. (2020b).

loss estimation based on the spectral response of the monitored PV material and the spectral irradiance conditions.

Because of its spectral transmittance profile, soiling induces higher spectral losses in high bandgaps PV technologies, such as a-Si and CdTe (John et al., 2016; Qasem et al., 2014). This is due to the fact that the spectral response of higher bandgaps PV materials peaks at wavelengths shorter than lower bandgaps materials, where the soiling transmittance is lower. However, the spectral response is not the only characteristic of PV cells that can lead to dissimilar soiling losses for different PV materials. Researchers from PUC Minas, in Brazil, have shown that the temperature can dominate the spectral effects, because of the different temperature coefficients of the various PV materials (Costa et al., 2019; Duarte et al., 2020). In particular, from the results of their analysis, supported by experimental data, the authors concluded that, under operating temperatures >40°C, higher bandgaps technologies (such as CdTe) still showed better performance compared with silicon, despite of the higher spectral losses.

The OSM sensors make use of small glass coupons to estimate the soiling losses of full-size modules. This approach has been occasionally questioned because of potential dissimilar soiling mechanisms that can take place on glass coupons and on the modules due, for example, to different temperature and dew cycles. However, glass coupons have been extensively used in the literature for PV soiling studies. Burton et al. (Burton et al., 2015) used field coupons to assess the optical effects and the mass distribution of soiling. Using a similar setup on a different location, Boyle et al. (Boyle et al., 2016) examined the airborne particles' deposition and mass accumulation on glass samples. Conceição et al. (Conceição et al., 2018b) used the glass coupons analysis to investigate the soiling losses of mono-crystalline Si modules. Toth et al. (Toth et al., 2018) and Einhorn et al. (Einhorn et al., 2019) discussed of the effectiveness of various cleaning strategies through the long-term analysis of glass coupons installed in five different locations. Nayshevsky et al. (Nayshevsky et al., 2019) used glass coupons to evaluate the self-cleaning effectiveness of a hybrid hydrophobic-hydrophilic coating that increases the dew collection rate and decreases the soil accumulation rates. Recently, Laarabi et al. (Laarabi et al., 2020) analyzed glass coupons installed in several different sites in Morocco and found a linear correlation between the deposited mass density and the transmittance losses. In addition, as mentioned earlier, the field comparison between the stand-alone-glass-based OSM sensors and the soiling stations is showing promising results (Gostein et al., 2019, 2020; Korevaar et al.,

2019; Morley et al., 2020). Despite that, specific analyses of the different soiling mechanisms occurring on stand-alone glasses and PV modules are recommended and should be conducted in future.

Soiling image analysis

In addition to OSM, it is possible to identify another still emerging class of soiling monitors that make use of image analysis. The soiling image analysis (SIA) sensors are distinct from the OSM, as they are designed to operate through the analysis of PV modules' aerial photos. Therefore, they do not directly measure the electrical loss (as soiling stations would do), do not make use of stand-alone glasses, and do not measure the optical properties of soiling (as OSM would do). Rather, they identify the area(s) of the modules' surface covered by soiling. As mentioned earlier, the area coverage can then be linearly converted into a transmittance loss (Figure 14). Pictures can be taken from drones (Mehta et al., 2018) or satellites (Supe et al., 2020) and analyzed through standard image processing or machine-learning techniques. In the recent years, researchers have proposed or investigated various image processing methods for soiling detection from modules' pictures (Mehta et al., 2018; Qasem et al., 2017; Supe et al., 2020; Yap et al., 2015). In addition, a novel SIA approach was recently proposed by Yang et al. (Yang et al., 2020a, 2020b). In this case, the brightness and the contrast of darker areas (cells) and of the lighter areas (ribbons and gaps) of the PV module's surface are compared. The soiling estimation is based on the measurement of the surface coverage, x, which is derived from the following equation:

$$x = \frac{1}{\sigma + \frac{R_d(1-BWR)}{BWR-R}} \quad \text{(Equation 3)}$$

where σ is the dust's attenuation coefficient of the brightness of the pattern, R is the ratio of the brightness of the unsoiled dark areas to the unsoiled light areas, R_d is the ratio of the brightness of the dust to the brightness of the unsoiled light areas, and *BWR* is the ratio of average brightness of the soiled dark areas to the soiled light areas. Of these parameters, R can be obtained from images of the clean surface, σ and R_d through model regression or artificial intelligence models, and *BWR* from images of the soiled surface. An indoor characterization of the setup is being conducted to validate the process and understand the effects of the camera settings (e.g. focus and exposure time).

Drones are becoming popular for the inspection of photovoltaic plants, as they can be equipped with infrared and/or electroluminescence cameras to detect in real time failures and defects of the PV modules (Jahn et al., 2018). However, their use might be unpractical or expensive if a constant monitoring of soiling is required. On other hand, if pictures of selected modules in the PV plant could be regularly taken, the SIA methodologies could be used for a continuous soiling monitoring, similarly to soiling stations and OSM devices. In addition, the SIA pictures could be used to analyze also the non-uniform distribution of soiling and, ideally, to model its effects on the electrical performance of the PV modules.

SOILING EXTRACTION ALGORITHMS

Soiling extraction algorithms are methods alternative to the installation of soiling monitors that can be used to detect the effect of soiling from a PV performance profile. In these cases, the PV modules themselves are converted into detectors. So far, they have been used for analysis of historical data, but they can be adapted to monitor also the current soiling losses and rates. At least two PV soiling extraction models have been presented in the literature and are here reported according to the naming used by (Deceglie et al., 2018a):

- The Fixed Rate Precipitation (FRP) (Kimber et al., 2007), which requires in input the PV performance metric and the rainfall pattern and generates a single soiling loss profile.
- The Stochastic Rate and Recovery (SRR) (Deceglie et al., 2018a), which requires in input only the performance metric and determines the average soiling ratio from a number of potential soiling profiles.

In the FRP model, a fixed soiling rate, measured from the derate of the longest dry period, is applied to any dry spell to generate a sawtooth-shaped soiling profile. The soiling ratio is set to 1 on any "valid" rainy day and for a number of days after it. These periods in which no soiling deposition occurs are known as "grace periods," but no definitive proof on whether they exist or not has been presented in the literature yet. In addition, rain events are considered "valid" only if they register daily accumulations above a predetermined minimum "cleaning threshold." In the original study, where 10 Californian sites were analyzed, cleaning thresholds between 0.2 and 0.4 inches/day (~5 and 10 mm/day) were considered. Various cleaning threshold values have been suggested and/or employed in the literature, expressed as accumulated rain

Table 2. Summary of the different cleaning thresholds used in the literature

Cleaning threshold	Notes	Climate conditions	Reference
5 mm/day		Tropical and subtropical desert climate (Bwh)	(Hammond et al., 1997)
1 mm/day		Mediterranean climate (Csb)	(Caron and Littmann, 2013)
4-5 mm/day	Tracked PV system	Temperate oceanic climate (Cfb)	(García et al., 2011)
3.5 mm/day	50% cleaning probability	Tropical and subtropical desert climate (Bwh)/ hot-summer mediterranean climate (Csa)	(Gostein et al., 2014)
5 mm/day		Tropical and subtropical desert climate (Bwh)	(Gostein et al., 2015)
1 mm/day		Mediterranean climate (Csb)	(Besson et al., 2017)
1 mm/day		Multiple locations, mainly mediterranean climate (Csb)/hot-summer mediterranean climate (Csa)	(Micheli et al., 2019a)
10 mm/day 5mm/day	80% of particles cleaned by > 10mm/day 30% of particles cleaned by < 5mm/day	Multiple locations, humid subtropical climate (Cfa)/tropical and subtropical desert climate (Bwk)/mediterranean climate (Csb)/hot-summer mediterranean climate (Csa)	(You et al., 2018)
8 mm/h	<5 mm/h did not cleaned the modules	Mid-latitude steppe and desert climate (Bsh)	(Valerino et al., 2020)
2.54–7.62 mm/day	Finer particles are not cleaned by rainfall	Tropical and subtropical steppe climate (BSk)	(Toth et al., 2020)
2.2 mm/day	50% cleaning probability	Hot-summer mediterranean climate (Csa)	(Conceição et al., 2020)
5 mm/h	<1 mm/h—no cleaning >5 mm/h—fully cleaned (additional thresholds considered for individual aerosols components and partial cleanings)	Worldwide	(Li et al., 2020)
0.01 mm/h and 1 mm/day		Hot-summer mediterranean climate (Csa)	(Micheli et al., 2021)

The climate conditions are sourced from the Köppen-Geiger climate classification (Kottek et al., 2006).

(in mm or inches) per day or per hour, depending on the available rain data. These range from 1 mm/day to >5 mm/day or to 8 mm/h and are summarized in Table 2. In addition, Gostein et al. (Gostein et al., 2015) reported that, studying a site in Southwestern USA, non-uniform corner soiling was not cleaned in one occasion by a 5 mm/day rainfall event, even if, in other occasions, more severe soiling was removed by rain events of slightly higher intensities. In this light, Javed et al. (Javed et al., 2020) have proposed a "relative recovery of cleanness index" to quantify the cleaning effectiveness of a rainfall event, dependent on both the specific rainfall intensity and the time passed since the previous rainfall.

The results of the FRP extraction can vary more or less significantly depending on the chosen inputs and in particular on the cleaning threshold. In addition, it should be noted that also the rain data source can affect the soiling extraction (Coello and Boyle, 2019).

The SRR model was developed with the aim of reducing the number of arbitrary choices in soiling extraction and of eliminating the dependence on rainfall data and cleaning logs. Indeed, this method does not require any weather data as inputs, because cleanings are identified based on positive shifts of the performance metric. The model calculates the running median of the performance metric and then follows four steps. First, the differences (Δ) between neighboring daily soiling ratio values are calculated and any positive shift larger than $Q_3+1.5\cdot IQR$ is identified as a cleaning, where Q_3 and IQR are respectively the third quartile and the interquartile range of all the $|\Delta|$ values. Second, the soiling rate of each period within two consecutive cleaning events is determined according to the methodology presented in Deceglie et al. (2018b). Third, a Monte Carlo simulation is performed, by stochastically generating 1000 possible soiling profiles. The soiling ratio of the first day following a cleaning is randomly selected from a half-normal distribution, not to assume necessarily a complete soiling ratio recovery. Fourth and last, the median of the average soiling ratios and the confidence intervals of the

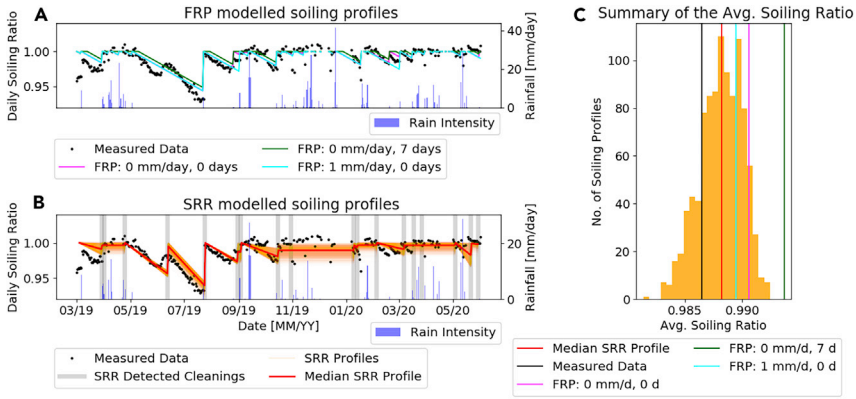

Figure 16. Comparison of soiling extraction models

(A) FRP modeled soiling profiles for three combinations of cleaning thresholds (0 or 1 mm/day) and of grace periods (0 or 7 days).

(B) SRR-modeled soiling profiles (in light orange). The median soiling profile is shown in red. The vertical gray lines represent the detected cleaning dates.

(C) Mean measured soiling ratio (black vertical line), mean of the FRP profiles (cyan, purple and green vertical lines), mean soiling ratio of the median SRR profile (red vertical line), and distribution of the average soiling ratios of the SRR generated soiling profiles (orange bars). Differently from the original version, in this case the irradiance weighting has been neglected in the SRR.

1000 profiles are calculated. The model was validated against the measurements of 11 soiling stations installed in the USA and returned lower errors than the FRP (Deceglie et al., 2018a). A Python version has been made available on GitHub by the authors (National Renewable Energy Laboratory, 2018b).

This weather-unaware approach has the advantage of not requiring the understanding of natural cleaning mechanisms, nor the knowledge of the operation and maintenance (O&M) schedule, which might be imperfectly reported or difficult to obtain. Indeed, as mentioned, not all rainfall events have cleaning effects and, in addition, parameters other than rain can wash off soiling. However, although this method does not require knowledge of the precipitation and considers different soiling rates for each dry period, it does not return a single daily soiling profile, but rather a distribution of potential average annual losses. In order to overtake this issue, and to develop an algorithm to analyze at the same time soiling and PV degradation, some of the authors (Deceglie et al., 2019) have proposed to extract the median daily soiling ratio profile from all the Monte-Carlo-generated profiles.

Figure 16 shows the profiles extracted through the two aforementioned methods from the short-circuit current data measured by the soiling station in Jaén. Different combination of cleaning thresholds and grace periods are tested for the FRP method (Figure 16A). In Figure 16B, it is possible to see the automatically determined cleaning dates (vertical gray lines) and the 1000 soiling profiles generated by the SRR method (orange lines). It is worth mentioning that the SRR detects the partial cleaning occurring between May and July 2019, which is not due to a rain and therefore not modeled by the FRP.

Some researchers have proposed modifications or have employed slightly modified versions of these methods. The use of monthly mean soiling rates rather than a fixed soiling rate was proposed to represent better the soiling seasonality in FRP (Micheli et al., 2020a). Skomedal et al. (Skomedal et al., 2019) proposed to modify the SRR cleaning detection equation in conditions of high data noise to $\delta\,(Q_3 + IQR)$, with δ being a site-specific parameter. In addition, they introduced some additional filters to remove outliers. A team from GroundWork Renewables, Inc. (Morley et al., 2020) suggested the addition of a GHI threshold to remove outliers from the performance metric before the SRR extraction. Last, the introduction of change points in addition to cleaning events to model sudden changes in soiling deposition rates within a dry spell has been suggested and is being investigated (Micheli et al., 2020c).

The main challenge of soiling extraction is represented by the calculation of the performance metric. In particular, the effects of non-soiling related issues affecting the PV performance have to be identified and removed.

These include, for example, PV module and inverter degradation and failures. In a recent work, Skomedal and Deceglie (Skomedal and Deceglie, 2020) proposed a method, named Combined Degradation and Soiling (CODS), to estimate simultaneously degradation and soiling losses. This makes use of the SRR cleaning event detection method and of the Kalman filter (Labbe, 2016) to estimate the soiling profile. In addition, spectral, angular and temperature-induced losses have to be corrected while extracting soiling from PV performance data. Most of these corrections can be performed through referenced methodologies (King et al., 2004). However, the weather data sources and the models used in the analysis have been found to affect the quality of the extraction (Defreitas et al., 2019) and should be selected with care.

ESTIMATION OF SOILING FROM ENVIRONMENTAL PARAMETERS

As mentioned, soiling of a PV plant is caused and can be affected by a number of factors, including environmental conditions, site characteristics, and system configuration. In particular, the variability of environmental parameters and their interaction play a key role in soiling deposition and removal. If the correlations between soiling and these parameters were known, it would be possible to estimate soiling without the need of soiling detectors and the analysis of PV performance. In addition, it should be noted that ground-based and/or satellite-derived environmental parameters' series are typically available for more locations and longer time intervals than PV data series. This means that, knowing the correlations between soiling and environmental parameters would make it possible to estimate, in advance, the soiling losses during the design, the cost evaluation, and the site selection phases of any new PV installation. For these reasons, there have been several studies that investigated the correlations between soiling losses and environmental parameters, which are summarized in Table 3.

The investigations on the correlations between soiling and environmental parameters have been following one of these two directions: estimation of average/annualized soiling losses or estimation of daily soiling losses. In the first case, the aim of the studies is to rank different locations depending on the severity of the average soiling loss experienced during long-term periods (one or more years). The results of this type of investigations can be used to estimate the impact of soiling on the yearly energy yield of a PV site and for the creation of soiling maps. Differently, the second class of investigations aims to predict the daily soiling profile through environmental parameters, identifying therefore cleaning events' dates and the soiling rates' values.

From the investigation of the average losses at several sites in the United States (20 sites in 2017 and 41 sites in 2019), it was possible to identify the key soiling predictors from a list of more than 100 variables (Micheli et al., 2019b; Micheli and Muller, 2017). The analysis showed that only the particulate matter and some parameters describing the precipitation pattern had significant linear correlations with the soiling metrics. In particular, the average and the maximum number of days in between rainfalls were found to be more important than the average intensity of the rainfalls for the estimation of soiling (Mejia and Kleissl, 2013; Micheli and Muller, 2017). In addition, it was also demonstrated that the way the particulate matter concentration data were sourced and processed could affect significantly the estimation (Micheli et al., 2019b). Compared with ground measurements, satellite-derived concentrations were found to return lower correlations with soiling, probably because biased by the non-uniform vertical distribution of aerosols in the Western and Central United States (Li et al., 2015). Nonetheless, a linear correlation has been reported by a different study (Cordero et al., 2018) between annual Aerosol Optical Depth estimates (ground measured in some cases and satellite retrieved in other cases) and annual average soiling rates measured in six Chilean locations.

On the other hand, the prediction of short-term soiling losses is more difficult than the estimation of annualized losses because the variability of the environmental parameters becomes more relevant than their average value. For a better visualization, a daily soiling profile can be generally approximated to a sawtooth wave, made of the alternation of soiling accumulation periods (in which the soiling loss increases) and cleaning events that cause an instantaneous drop of the losses. Each environmental parameter can have an effect on the accumulation (varying the slope of the profile) or on the removal of soiling (causing a soiling ratio recovery), or on both the processes. The following subsection provides an overview of the mechanisms that cause and affect the deposition and the removal of soiling from PV surfaces. This subsection does not want to be a full in-depth review of the soiling mechanisms, which have been extensively described elsewhere (Figgis et al., 2017; Ilse et al., 2018). Rather, this aims to be a summary that will help understand the scientific backgrounds of the estimation models described in "soiling deposition and removal mechanisms".

Table 3. Summary of the studies investigating the correlations between soiling and environmental parameters

Reference	Year	Location	Climate	Variables	Findings
Kimber et al., 2007	2007	Southwest of the USA	Dry-summer subtropical	Rain	Soiling losses can be modeled assuming a linear degradation rate within each dry period.
Cabanillas and Munguía, 2011	2011	Sonora, Mexico	Tropical and subtropical desert climate	Particle size	The most numerous particles were of 52 μm size. 20 μm size particles represented the largest fraction of the total deposited volume.
Boyle et al., 2013	2013	Colorado, USA	Tropical and subtropical steppe	PM (mass accumulation)	Experimental investigation on the soiling mass accumulation and on its correlation with the transmittance losses. Each g/m^2 of dust accumulated on a glass surface caused a 5.8% decrease in power output.
Mejia and Kleissl, 2013	2013	California, USA	Dry-summer subtropical	Rain	Soiling losses increase linearly between rain events. Average soiling rate of 0.051%/day on a summer dry period.
Boyle et al., 2014	2014	Colorado, USA	Tropical and subtropical steppe	PM (deposition velocity)	Correlation between the PM values and the mass accumulation. Average V_d of 2.5 cm/s and 2.01 cm/s were found for the two studied sites.
Csavina et al., 2014	2014	Arizona, USA, and Chihuahua, México	Tropical desert, tropical and subtropical steppe	PM, WS, RH	Spearman correlation between RH and PM_{10} at WS > 4m/s has a coefficient of −0.66.
Weber et al., 2014	2014	Mexico City, Mexico	Oceanic subtropical highland	PM, rainfall	Dry periods, together with the deposition rate, could be used to predict of soiling losses. Average deposition rates observed in this location were 65 g m^{-2} day^{-1}.
Guo et al., 2015	2015	Doha, Qatar	Tropical and subtropical desert climate	PM, WS, RH	Daily change of Cleanness Index (ΔCI) was negatively correlated with PM and RH, and positively correlated with WS. $\Delta CI = 2.3 * 10^{-3} - 5.7 * 10^{-2} * PM_{10} + 3.5 * 10^{-3} * WS - 2 * 10^{-1} * RH$
Boyle et al., 2016	2016	Colorado, USA	Tropical and subtropical steppe	PM (mass accumulation)	Comparison between dry dust deposition on glass samples and ambient PM concentrations. Mean V_d of 2.14 cm/s and 2.12 cm/s for the two studied sites.
Figgis et al., 2016b	2016	Doha, Qatar	Tropical and subtropical desert climate	PM, RH, WS, soiling deposition and removal rate, particle size	Deposition depended mainly on WS and was almost independent of RH and PM_{10}. Almost no resuspension occurred for RH>80%. Most of resuspension occurred at high WS and low RH.

(*Continued on next page*)

Table 3. *Continued*

Reference	Year	Location	Climate	Variables	Findings
Kim et al., 2016	2016	USA, Indoor experiment	–	RH, surface and particle properties, resuspension rate	Resuspension rates are affected by RH and surface properties. On glass surfaces, at low RH, resuspension rates were in the order of 10^{-3} s^{-1}. The rate started to reduce at around 50%/60% RH and then decrease by 2x at 70% RH.
Mani et al., 2016	2016	Rajasthan, India	Hot semi-arid climate	Particle size, tilt angle	The correlation between soiling losses, particle composition, and tilt angles are investigated. Optimal tilt angles are recommended for the site depending on the particle size.
Javed et al., 2017a	2017	Doha, Qatar	Tropical and subtropical desert climate	PM, WS, RH	Higher PM_{10} concentrations led to higher soiling deposition rates at low WS and RH. No significance for PM_{10} at high WS (>4 m/s) and high RH (>65%). Soiling losses lowered for higher WS and low RH.
Micheli et al., 2016	2017	Multiple cities, USA	Tropical, temperate and arid	PM, WS, RH, and rainfall	Investigated the correlation of soiling with climate classification, PM, and average length of dry periods.
Micheli and Muller, 2017	2017	Multiple cities, USA	Arid, temperate and equatorial	PM, rainfall, wind direction	At shorter distances, PM_{10} and $PM_{2.5}$ showed similar correlations with average soiling losses. At longer distances, $PM_{2.5}$ acted better than PM_{10}. A two variable regression with PM and the average length of the dry period showed a correlation with R^2 of 0.9.
Bergin et al., 2017	2017	India, Central China and Arabian Peninsula	Mid-latitude steppe and desert, humid subtropical, tropical and subtropical desert	PM	Showed the influence of each component of PM on the transmittance losses and proposed a method to model the soiling loss, which makes use of mass loading, absorption, and scattering efficiency and PM upscatter fraction. Also found that PM mass was dominated by dust (92%), but the non-dust PM fraction, instead, was responsible of 50% of reduction in transmittance.
Etyemezian et al., 2017	2017	Nevada, USA	Tropical and subtropical desert climate	Wind	Investigated the effect of the mean wind flows on a PV system. Reduction of the friction velocity up to 90% found for wind angles of 150°–180°.

(*Continued on next page*)

Table 3. *Continued*

Reference	Year	Location	Climate	Variables	Findings
Micheli and Deceglie, 2018	2018	Multiple cities, USA	Tropical, temperate, and arid	PM, rainfall	Investigated the possibility of using historical environmental parameters data to predict future soiling losses.
Micheli et al., 2019b	2018	Multiple cities, USA	Equatorial, temperate, and arid	PM, rainfall, WS, wind direction, distance between stations, length of dry periods	Extension of (Micheli and Muller, 2017) using data from more soiling stations. Size of PM, distance between soiling stations and PM monitors, and the interpolation method found to affect the correlation between soiling and PM.
Figgis et al., 2018	2018	Doha, Qatar	Tropical and subtropical desert climate	PM, RH, WS, deposition and removal rate	Deposition mostly influenced by WS, with a linear increase starting at 3 m/s. Rebound mostly affected by WS (start to decrease at 4 m/s); RH did not have strong impact. Small significant correlations between resuspension, WS, and RH. Net accumulation more influenced by WS.
You et al., 2018	2018	Taiwan, Japan, China, USA, Spain, Qatar and Australia	Multiple climate	PM, rainfall, RH	Soiling estimated from particle matter and deposition velocities and used to determine optimal cleaning frequency. Longest optimal cleaning interval for Malibu, USA (70 days for manual cleaning) and the shortest interval for Doha, Qatar (23 days for manual cleaning).
Conceição et al., 2018a	2018	Évora, Portugal	Hot-summer mediterranean climate	Rain, aerosol optical depth (AOD), mass accumulation	Showed the decrease of r_s due to Saharan dust storms and pollen. Highest dust concentration during a dust storm event reached 900 $\mu g/m^3$.
Coello and Boyle, 2019	2019	Arizona and California, USA	Tropical and subtropical steppe climate/dry-summer subtropical	PM, deposition velocity	Model to convert PM concentrations into soiling losses. Best results obtained when using settling velocity rather than deposition velocity: 0.4 cm/s for $PM_{10-2.5}$ and 0.09 cm/s for $PM_{2.5}$.
Ilse et al., 2019a	2019	Doha, Qatar	Tropical and subtropical desert climate	Dew	Investigation on the influence of dew in the soiling processes (cementation, capillary aging and particle caking). Soiling found to lower if the surface is heated.

(*Continued on next page*)

Table 3. *Continued*

Reference	Year	Location	Climate	Variables	Findings
Figgis et al., 2019	2019	Doha, Qatar	Tropical and subtropical desert climate	Wind, dust accumulation, dust deposition	Soiling deposition decreased as the WS increased in wind tunnel tests. Highest decrease at 4 m/s. Field tests showed that the dust accumulation lowers for surfaces facing toward the wind, compared with facing downwind at the same tilt angle.
Isaifan et al., 2019	2019	Doha, Qatar	Tropical and subtropical desert climate	PM, relative humidity	Showed that the fraction of the PM_{10} depositing on a PV panel surface changes depending on the relative humidity. The correlation between PM and the performance ratio have an $R^2 = 0.94$ when using only the sticky-fraction of the airborne particulate matter concentration.
Valerino et al., 2020	2020	Gandhinagar, India	Mid-latitude steppe and desert climate	PM, rain, and RH	Rainfalls >8 mm/h can clean the modules, whereas light rain (<5 mm/h) and high RH levels can increase the PM deposition velocity and the soiling rate. In the rainless period, the average PM_{10} concentrations were 2.5x greater but soiling rate was 2x lower.
Toth et al., 2020	2020	Colorado, USA	Tropical and subtropical steppe climate	PM	Model to predict soiling on a daily basis using PM fine and PM coarse data. The cleaning threshold was determined so that it optimized the modeling results. It provides evidences that low-cost PM sensors can be good options for PV soiling modeling.
Sanz Saiz et al., 2020	2020	Madrid, Spain	Mediterranean climate	Pollen	A linear correlation between the transmittance losses and the density of artificially deposited pollen was found. Non-uniform soiling patterns were observed after a light rain.
Javed et al., 2020	2020	Doha, Qatar	Tropical and subtropical desert climate	PM, rain, WS, and RH	The average soiling rate increased with PM, RH, and dust storms frequency and decreased with WS and rain frequency. A methodology is proposed to evaluate the cleaning effectiveness of rain events

Acronyms used in this table: PM (Particulate Matter); RH (Relative Humidity); V_d (Deposition Velocity); WS (Wind speed). The climate information were sourced from the Köppen-Geiger climate classification (Kottek et al., 2006).

Table 4. Estimations of transmittance losses ($\Delta\tau$) or PV energy losses (ΔE) based on the total mass accumulation (ω)

Reference	Equation	Notes	Method
Hegazy, 2001	$\Delta\tau(\%) = 1 - 34.37 \cdot erf(0.17 \cdot \omega^{0.8473})$		1-year exposure of glass samples in Egypt.
Elminir et al., 2006	$\Delta\tau(\%) = 0.0381 \cdot \omega^4 - 0.03626 \cdot \omega^3 + 6.4143 \cdot \omega^2 - 15.051 \cdot \omega + 16.769$	For $1.5\ g/m^2 \leq \omega \leq 9\ g/m^2$	Exposure of glass samples in Egypt.
Kaldellis and Kapsali, 2011	$\Delta E(\%) = e^{-A_{eq} \cdot \omega}$	A_{eq}: mass content coefficient	Artificial deposition of ash, limestone, and red soil on PV modules.
Jiang et al., 2011	$\Delta E(\%) = 0.0139 \cdot \omega$		Artificial deposition of ISO 12103-1 A2 test dust on PV modules.
Boyle et al., 2013	$\Delta\tau(\%) = 0.058 \cdot \omega$		Exposure of glass samples over 1 year and a half in Colorado.

Soiling deposition and removal mechanisms

The rate at which soiling accumulates on the PV modules' surface (*Accumulation*) is the result of three phenomena (Ilse et al., 2018):

$$Accumulation = Deposition - Rebound - Resuspension \quad \text{(Equation 4)}$$

where *Deposition* is the rate at which particles impact on the surface; *Rebound* is the rate at which particles immediately bounce off from a surface without adhering; and *Resuspension* is the rate at which particles, after an initial adhesion, are removed from the surface (Figgis et al., 2017; Ilse et al., 2018). A review specifically focused on the factors impacting each phenomena, briefly described here, can be found in (Figgis et al., 2018).

The first important factor affecting the deposition processes is the concentration of suspended particles in the atmosphere. As shown in Table 4, researchers have reported correlations between mass accumulation and soiling or transmittance losses, using different sets of data (Boyle et al, 2013, 2015; Burton et al., 2015; Elminir et al., 2006; Hegazy, 2001; Jiang et al., 2011; Kaldellis and Kapsali, 2011). A comparison of these models is not currently possible, as these were developed for different conditions and glass surface designs and configurations. However, comparative studies should be conducted in future.

Although in most cases the soiling accumulation has been estimated from the particulate matter (PM, see "experimental setup" for a definition) because of its wide availability, some authors have highlighted that PM_{10} and $PM_{2.5}$ only represent a fraction of the particle distribution. This means that, in some cases, soiling particles can be bigger than those included in the PM indexes (Cabanillas and Munguía, 2011; Javed et al., 2017b; Mani et al., 2016; Roslizar et al., 2020; Valerino et al., 2020). However, Valerino et al. (Valerino et al., 2020) reported that, even if large particles are dominant in terms of deposited mass, the soiling losses are mainly caused by the small particles. Nonetheless, Isaifan et al. (Isaifan et al., 2019) showed that only a fraction of the suspended PM_{10} deposits on the PV module surface and the so-called PM_{10} sticky-fraction is correlated to the relative humidity through a modified sigmoid function with an inflection point at 70% RH. Above this value most of the PM is deposited, due to the action of capillary forces.

In addition, other environmental parameters can affect the deposition rate of the suspended particles. For example, Javed et al. (Javed et al., 2017a) showed that the impact of particulate matter on soling is strongly dependent on the weather conditions: in Doha, Qatar, the PM_{10} was found to have a significant effect on soiling (p value < 0.05) only for relative humidity (RH) < 50%. In addition, Figgis et al. (Figgis et al., 2018) found a poor correlation between deposition rate and the PM_{10} at low/moderate PM concentrations, whereas the deposition rate increased significantly for high PM_{10} concentration conditions (>1000 $\mu g/m^3$). In the same work, they also found that wind speeds (WS) > 3.5 m/s led to an increase in size of deposited particles and not necessarily led to an increase in particle concentrations.

In addition to the particulate matter, also organic contaminants have been reported to contribute to soiling, at least in certain regions and in determined seasons. Subaerial biofilms, including fungi, were first found deposited on PV modules installed in Sao Paulo, Brazil (Shirakawa et al., 2015). Subsequent investigations reported the presence of hard-to-remove filamentous fungi on glass coupons installed for one year in Sacramento, CA (Toth et al., 2018) and in Mumbai, India (Einhorn et al., 2019). Even pollen can cause losses: its presence was reported for PV modules in Belgium (Appels et al., 2013) and in Southern Portugal (Conceição et al., 2018a). In particular, in this last work, the authors showed a soiling accumulation twice as high in the high-pollen spring compared with summer. Wagner and Vogel (Wagner and Vogel, 2019) reported that, during the pollen season, the soiling rate in Karlsruhe, Germany, increased from a background value of 0.001%/day up to 0.5%/day. Recently, a team from CIEMAT in Spain (Sanz Saiz et al., 2020) found a linear correlation between the average transmittance loss (τ, calculated in the 0.3–1.2 μm range) and the density of cypress pollen (ω in g/m^2) artificially deposited on glass coupons:

$$\tau\,(\%) = 99.7\% - 3.8\%\cdot\omega \qquad \text{(Equation 5)}$$

However, probably driven also by the lack of concentration data availability, the knowledge on the impact of pollen on PV is quite limited. In addition, because of its size, typically ranging from 15 μm to 200 μm (Pacini, 2015), pollen is not generally included in PM_{10} or $PM_{2.5}$ measurements.

Wind can have a double effect on soiling, as it can favor deposition, but it can also enhance rebound and resuspension. For example, Javed et al. (Javed et al., 2020) observed that soiling was lower in the dry and windy season, because of the enhanced resuspension, compared with other dry periods in different seasons. In addition, natural cleanings events can occur because of high winds (Javed et al, 2017a, 2020). A 51-day long experimental study conducted by Figgis and colleagues (Figgis et al., 2018) was concluded as follows:

- Wind was among the governing factors of the deposition process. In particular, the deposition was found to increase significantly for wind speeds >3.2 m/s.
- Wind was the only responsible agent for particle rebound. The rebound rate was found to increase linearly with the wind speed, at least up to wind speeds of 4 m/s.
- Wind could cause small variations in resuspension rates. On the other hand, wind gusts were found responsible for significant resuspension from PV modules (Guo et al., 2015). Ilse et al. (Ilse et al., 2018) reported that natural cleanings took place at wind speeds >3 m/s, with a significant increase above 4 m/s.

Also the relative humidity can have effects on soiling accumulation. Relative humidity strengthens the capillary adhesion of particles to the surface and is the dominant factor affecting the resuspension rate (Figgis et al., 2018). In addition, condensation increases dust accumulation (Ilse et al., 2019a; Naumann et al., 2018). Condensation was found to occur at night also for RH as low as 60%, probably because the radiative cooling brought the module temperature below the dew point temperature. For this reason, the nighttime heating of the PV modules has been proposed as potential soiling mitigation solution (Ilse et al., 2019b). On the other hand, dew can also have cleaning effects on the PV modules, especially on tilted surfaces (Gostein et al., 2019, 2020).

In most sites, the most common natural cleaning events are rainfalls (Kimber et al., 2007), even if, as discussed earlier, not all the rain events have been found to wash off soiling and there is an on-going discussion on the value of a minimum cleaning threshold (Table 2). In addition, light rain events can have effects similar to those of high RH, leading to increased soiling deposition rates (Naeem and Tamizhmani, 2016; Valerino et al., 2020). In regions with limited rainfall, such as Qatar, wind was found to be the dominant natural cleaning process (Ilse et al., 2018).

It should be noted that conditions external to weather, pollution, and climate also have an effect on the soiling deposition rate. For example, it is known that steeper tilt angles reduce the soiling losses (Cano et al., 2014; Conceição et al., 2019b) and different orientations with regard to the wind can change the deposition and accumulation rates (Figgis et al., 2019). The dissimilar effects of soiling on different PV technologies have already been discussed in "optical soiling measurement" (John et al., 2015; Qasem et al., 2014). Other soiling influencing factors include, but are not limited to, the deposition of anti-soiling coatings (Ilse et al., 2019b), the tracking configuration (García et al., 2011), the presence of a frame (Gostein

Table 5. Summary of the supporting equations for the presented models (Bergin et al., 2017; Coello and Boyle, 2019)

Parameter	Equation	Arguments	Reference
Aerodynamic resistance	$R_a = \frac{\ln\left(\frac{Z_R}{Z_0}\right) - \psi_H}{k u_*}$	Z_R is the reference height in which the v_d is evaluated, Z_0 is the roughness length, ψ_H is the stability function, k is the Von Karman constant, u_* is the friction velocity.	Coello and Boyle, 2019
Friction Velocity	$u_* = \frac{\kappa \bar{u}_x(h_r)}{\ln\left(\frac{h_r}{Z_0}\right)}$	κ is the Boltzmann's constant, $\bar{u}_x(h_r)$ is the wind speed at the reference height h_r	Coello and Boyle, 2019
Mass absorption efficiency	$E_{abs,i} = \frac{\frac{3}{2}Q_{abs}}{\rho_p D_p}$	$Q_{abs,i}$ Mie absorption coefficient, ρ_p is the particle density, D_p is the average particle diameter.	Bergin et al., 2001
Mass scattering efficiency	$E_{scat,i} = \frac{\frac{3}{2}Q_s}{\rho_p D_p}$	$Q_{s,i}$ Mie scattering coefficient, ρ_p is the particle density, D_p is the average particle diameter.	Bergin et al., 2001
Quasi-laminar layer resistance	$R_s = \frac{1}{3u_* R_1 (E_B + E_{IM})}$	E_B and E_{IM} are the collection efficiencies from Brownian diffusion and impaction, R_1 is the correction factor of particles that stick at the surface.	Coello and Boyle, 2019
Settling velocity	$v_s = \frac{\rho_p D_p^2 g}{18\mu}$	ρ_p is the particle density, D_p is the particle diameter, g the gravitational acceleration, μ is the dinamic viscosity of the air.	Coello and Boyle, 2019

et al., 2015), or the height at which the PV modules are installed (Karim et al., 2018). Nonetheless, a number of investigations have presented models that can allow monitoring the daily soiling losses using environmental parameters. These models are discussed in the following section.

Soiling estimation models

Most of the models presented so far are based on the particulate matter. Using the data collected at five locations in the USA, Boyle (Boyle, 2015) proposed the following equation to estimate the loss in transmittance:

$$\Delta\tau = 0.22 + 0.005 \cdot \sum_{d}^{n} TSP_d \qquad \text{(Equation 6)}$$

where TSP_d is total suspended particles (diameter <100 μm) on the day d and n is the number of days since the soiling deposition started.

Using the performance of PV modules installed in Ahmedabad, India, Bergin et al. (Bergin et al., 2017) proposed an equation to describe the loss in the optical transmittance per unit of deposited mass from the PM concentration:

$$\frac{\Delta\tau}{PM_F} = -\frac{1}{PM_F}\sum_{i=1}^{n}(E_{abs,i} + \beta_i E_{scat,i}) \cdot PM_{F,i} \qquad \text{(Equation 7)}$$

where i represents the different particulate matter components, PM_F is the total mass loading, and $E_{abs,i}$, β_i, $E_{scat,i}$, and $PM_{F,i}$ are respectively the mass absorption efficiency, the PM upscatter fraction, the mass scattering efficiency, and the mass loading of the component i. The authors considered the PM is made of dust, organic carbon, elemental/black carbon, and "others" (sum of light scattering ions sulfate, nitrate, and ammonium). The equations used to determine $E_{abs,i}$and $E_{scat,i}$ are reported in the Table 5. This model assumes a linear relationship between the PM mass loading and the variation in transmittance. It was used initially to estimate the yearly soiling losses in Northern India (17%), Eastern Central China (17%), and the Arabian Peninsula (25%). More recently, Equation (7) was also employed to estimate the soiling losses worldwide (Li et al., 2020) through the use of long-term satellite-observation-constrained weather data and particle matter deposition rates sourced from the MERRA-2 reanalysis dataset.

You et al. (You et al., 2018) modeled the soiling loss occurring in seven cities worldwide by considering a loss in efficiency of 0.0139% per gram of dust deposited on a 1 m^2 of PV module surface, originally reported in Jiang et al. (2011). The dust deposition density (ω) was estimated as:

$$\omega = V_d \cdot TSP \cdot N_D \cdot 10^{-6} \quad \text{(Equation 8)}$$

where V_d is the deposition velocity, TSP is the Total Suspended Particulates (size ranging between 20 and 50 μm), and N_D is the number of days without rainfall. The model returned variations up to five times in modeled deposition velocity compared with the experimental values reported in the literature. No definitive indication is reported on the electricity output uncertainty, other than an error of 3.4% in the estimation of the daily electricity output in January for one of the locations.

A similar method was proposed by Coello and Boyle (Coello and Boyle, 2019) and uses as inputs the PM_{10} and $PM_{2.5}$ concentrations, the rainfall data, and the tilt angle to estimate the soiling losses. The method starts with the estimation of the mass accumulation per time step (m, in $g \cdot m^{-2}$) for each dry period:

$$m = (v_{10-2.5} \cdot PM_{10-2.5} + v_{2.5} \cdot PM_{2.5}) \cdot t \cdot cos\theta \quad \text{(Equation 9)}$$

where v is either the deposition velocity or the settling velocity, PM is the daily average particulate matter concentration, t is the time step (in seconds), and θ is the tilt angle of the module surface. In this case, the particulate matter is grouped in particles of diameter between 10 and 2.5 microns ("*10–2.5*" subscript) and particles of diameter lower than 2.5 microns ("*2.5*" subscript). Three scenarios, each with a different parameter (variable deposition velocity, static deposition velocity, or static settling velocity) as v in Equation (9), were considered. The variable deposition velocity was calculated through the methodology presented in (Steinfeld and Pandis, 1998), as:

$$v = v_s + \frac{1}{R_a + R_s} \quad \text{(Equation 10)}$$

where v_s is the gravitational settling velocity or the Stokes velocity, $R_a$is aerodynamic resistance, and R_s is the quasi-laminar layer resistance (Table 5). The static deposition velocity was set to 9.17 and 1.5 cm s^{-1} for $PM_{10\text{-}2.5}$ and $PM_{2.5}$ respectively, based on observed values at different meteorological stations. Last, the static settling velocity was set to 0.4 and 0.09 cm s^{-1} for $PM_{10\text{-}2.5}$ and $PM_{2.5}$ respectively, based on a model presented by (Sehmel and Sutter, 1974). Each time series was generated as cumulative sum of the daily accumulations calculated from Equation (9), and the accumulation was reset for rainfalls of intensities above a minimum site-specific threshold. The soling ratio was then calculated using the equation proposed by (Hegazy, 2001) and shown in Table 4. The results of the investigation, based on the analysis of seven soiling station time series, showed that the static settling velocity model returned a profile similar to that of measured soiling, whereas the static and variable deposition velocity models overestimated the losses by factors of 10x and 5x, respectively.

More recently, Toth et al. (Toth et al., 2020) presented a model to predict daily soiling loss time series using rainfall, $PM_{10\text{-}2.5}$ and $PM_{2.5}$, based on the following equation:

$$r_s = 1.0 - (A_1 * F_d) - (A_2 * C_d) \quad \text{(Equation 11)}$$

where F_d is the cumulative sum of the $PM_{2.5}$ concentration since the first day of data collection, C_d is the the cumulative sum of $PM_{10\text{-}2.5}$ concentration since the last cleaning event, and A_1 and A_2 are constants fitted through the Truncated Newton (TNC) algorithm (Numerical Optimization, 2006). Interestingly, in this case natural rainfalls are assumed to be able to wash off coarse particles only ($PM_{10\text{-}2.5}$). The model was tested in an urban-industrial area in Colorado, considering the PM_{10} and the $PM_{2.5}$ measurements of a high-accuracy single-particle light scattering sensor (GRIMM EDM 180) and of a low-cost multiple-particle light scattering sensor (Dylos DC1100 PRO). The fitting returned A_1 and A_2 values of 1.8×10^{-5} and 3.5×10^{-5} $m^3/\mu g$, respectively for the GRIMM measurements and 2.6×10^{-7} and 1.4×10^{-5} ft^3 per thousand particles for the Dylos measurements. The model returned RMSEs of 0.013 and 0.014 when the one-year daily soiling loss profile was estimated using the GRIMM and the Dylos, respectively.

At least two investigations have attempted to model the daily soiling profile by taking into account a larger number of environmental parameters, in addition to particulate matter and rainfalls. Figgis et al. (Figgis et al., 2018) used an outdoor soiling microscope to collect soiling on greased and ungreased glass samples in a desert environment. The authors found the best modeling results for:

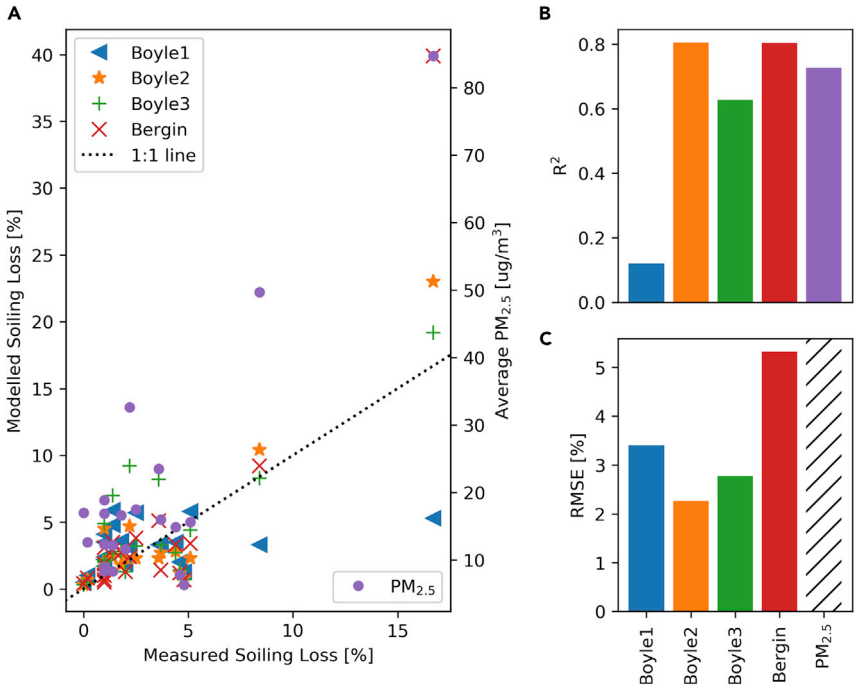

Figure 17. Estimation of soiling from environmental parameters

Measured and modeled average soiling ratio values reported by Pelland et al. (Pelland et al., 2018) for 20 sites worldwide (A). Coefficients of determination, R^2, (B) and RMSE (C) of each model are also shown. The models used in this work are those proposed by (Bergin et al., 2017; Boyle, 2015). Boyle1 uses dust surface mass concentrations from MERRA-2, Boyle2 the 2015 average and Boyle3 the July 2016–June 2017 PM_{10} data from the European Center for Medium-Range Weather Forecasts Copernicus Atmosphere Monitoring Service and Bergin the GISS Model E2 global climate model. In addition, average satellite-derived $PM_{2.5}$ concentrations for 2016 have been considered.

$$Accumulation = 10.6 - 4.99WS + 247PM_{10} - 73.4WS * PM_{10} - 14.9\Delta WS_{1hr} \quad \text{(Equation 12)}$$

where ΔWS_{1hr} is the difference between the current wind speed and the value recorded 1 h earlier. Equations to calculate the deposition, rebound, and resuspension rates were also reported in the same work. Javed et al. (Javed et al., 2017a) used artificial neural networks (ANN) to estimate a more than 2-year-long soiling profile in Qatar. An ANN with one hidden layer of 20 neurons returned significantly better performance in the estimation of the daily soiling losses compared with a multiple linear regression model (R^2 of 0.54 versus 0.17, respectively), given the same 10 variables in inputs (same and previous day PM_{10}, WS, RH, same day ambient temperature and wind direction, frequency of wind gustiness, and cumulative exposure time). In that work, the authors found it important to consider the frequency of wind gusts (>4 m/s) as an input variable, in addition to the average wind speed.

As described, most of these models are based on a single site. This opens questions regarding the universal applicability of the models. Pelland et al. (Pelland et al., 2018) compared the estimations of Boyle's and Bergin's models for 20 locations worldwide (Bergin et al., 2017; Boyle, 2015). Boyle's model was given in input: dust surface mass concentrations from MERRA-2 (here labeled as Boyle1) and both the 2015 average and the July 2016-June 2017 PM_{10} data from the European Center for Medium-Range Weather Forecasts Copernicus Atmosphere Monitoring Service (Boyle2 and Boyle3, respectively). Longer term soiling rate means, provided by the authors of (Bergin et al., 2017) and sourced from the GISS Model E2 global climate model, were instead inputted into the Bergin's model. Rainfall data from MERRA-2 were employed for both the models, using a threshold of 0.15 inches/day (~3.8 mm/day). The two models were used to calculate the long-term average soiling ratios of the 20 sites, and their estimations were compared with measured data. In addition to these models, considered in the original work, the average 2016 satellite-derived $PM_{2.5}$ concentrations from the V4.GL.02 database of the Dalhousie University (Van Donkelaar et al., 2016), calibrated to global ground-based observations, have been added in the present study. All the models, but Boyle1, were found to return $R^2 > 0.6$ with the best results for Boyle2 and

Table 6. Summary of PV soiling monitoring technologies and of their features and limitations

Technology	Description	Status	Features (+) & Limitations (−)
Soiling stations	Comparison of the electrical output of a soiling device and a clean PV device	Commercial	+ Standard monitoring solution + Directly measure the electrical impact of soiling − Require maintenance − Require human intervention (if not automatic) − Risk of missed or imperfect cleanings
Optical soiling measurement (OSM) detectors	Electrical loss estimation based on optical characterization of soiling	Early commercial In development	+ Low cost + Promising results from field validation − Ignore spectral losses − Use glass coupons instead of PV devices
Soiling image analysis (SIA) sensors	Soiling determined through the estimation of the area coverage from photos of the PV modules	Research	+ Quantify directly soiling on PV modules + Can detect non-uniform soiling + Potentially able to identify multiple defects and failure types − Expensive or impractical if constant monitoring is required − Effects of reflection, camera settings and shadings not clear
Extraction algorithms: Fixed rate precipitation (FRP) and stochastic recovery rate (SRR)	Soiling profile identified from PV performance time series	Available	+ Directly measure the energy impact of soiling + No detectors required − Require identification and elimination of non-soiling related issues − Subject to bias due to arbitrary choices in input (FRP) or to irradiance and temperature data sourcing and processing
Estimation models	Soiling profile generated from environmental parameters	Research	+ No soiling sensors required + Multi-year ground-based and/or satellite-derived datasets available + Make soiling forecast possible − Site specific − Lower accuracy − Ignore effects of system configuration and module design

Bergin ($R^2 > 0.8$), as shown in Figure 17. Using average $PM_{2.5}$ concentrations shows similar R^2 than the best daily estimation models. This is not surprising, as the models are used to calculate an average soiling ratio rather than the daily loss profile. Overall, Boyle2 and Boyle3 show the lowest RMSE (not calculated for $PM_{2.5}$ approach), with errors <3%. As acknowledged by the authors of the original study, the results are quite affected by the two points with losses >8%. More comparisons like this should be conducted to validate the performance of the various models in estimating the daily soiling loss profiles in different locations and for various environmental and soiling conditions.

OUTLOOK

In this work, several soiling monitoring technologies have been described. Their features and limitations are summarized in Table 6. Rather than disadvantages, these limitations should be considered as research and development opportunities.

The methodologies currently available to estimate soiling losses from environmental parameters have also been described. The main soiling predictors have already been identified by previous works (Table 7), but additional research is needed as most of the studies are site specific and the effect of some factors, such as the presence of a frame on the module or the tilt angle, still has to be modeled. However, historical time

Table 7. Research directions and best predictors in the estimation of soiling losses through environmental parameters

Target	Main Predictors
Long-term average losses	Particulate matter & average and maximum length of dry periods.
Daily soiling loss values	Particulate matter; wind speed; relative humidity; rainfall.

series of the environmental parameters are widely available and can therefore be ideally used to estimate soiling losses of any site, even if no PV data are available.

Some of these monitoring solutions require a purchase and installation cost (soiling stations, OSM detectors, and SIA sensors), whereas others can be ideally put in place at no cost. Indeed, soiling extraction, in its easiest form, only requires in input a performance ratio, which is typically calculated even at those sites where no soiling mitigation is done. When not available, satellite-derived irradiance and temperature data can be sourced for any locations either for free or for a fee.

In general, one would expect the soiling monitoring costs to be covered by the profits made through soiling mitigation. In their global assessment work, Ilse and coauthors (Ilse et al., 2019b) estimated the maximum allowed cost for soiling mitigation at utility scale PV plants. This value, in €/m^2, expresses the maximum expenditure that can be made to mitigate soiling and achieve a positive net present value (NPV). Its value depends on the effectiveness of the soiling mitigation (i.e. the percentage reduction in soiling accumulation rate) and was calculated assuming optimum cleaning cycles, power purchase prices of 0.03 €/kWh, and a 10-year payback period for technology investment at 5% discount rate (Ilse et al., 2019b).

The maximum allowed costs calculated by (Ilse et al., 2019b) can be used also to determine the maximum allowed costs for soiling monitoring. The main challenge, however, is represented by the need of determining which percentage of the mitigation costs can be used for soiling monitoring. The following analysis takes into account two possible monitoring costs scenarios:

i. Considering a 10-year payback period, monitoring costs are equal to an eleventh (9.09%) of the maximum allowed costs for mitigation. So the maximum allowed costs are equally divided between the purchase of soiling monitors (occurs only once) and each of the 10 years in which soiling mitigation is performed.

ii. Monitoring uses the 90.9% (10/11) of the maximum allowed costs for mitigation.

The original investigation showed that the allowed mitigation costs increased with the efficacy of the mitigation: a larger reduction in soiling rates obtained through mitigation makes it possible to increase the mitigation expenditure. So, two mitigation costs scenarios have been considered in this case:

i. Mitigation costs = 0.5 €/m^2. This is the allowed mitigation costs calculated by (Ilse et al., 2019b) to reduce the soiling rate by 20%.

ii. Mitigation costs = 1.3 €/m^2. This is the allowed mitigation costs calculated by (Ilse et al., 2019b) to reduce the soiling rate by 50%.

From these two values, it is possible to calculate the maximum allowed mitigation cost per each power plant and therefore the maximum allowed monitoring cost in each scenario. The maximum allowed monitoring cost is then divided by the number of sensors per plant, determined accordingly to the standards (International Electrotechnical Commission, 2017), to calculate the maximum allowed cost per sensor for each PV plant. This procedure is repeated for each site in the five countries considered in the market analysis of 4.3. The mean maximum allowed monitoring cost and the 95% confidence interval are reported in Table 8, where PV plants are grouped by size. A PV module efficiency of 18.1% (Canadian Solar Inc CS3K-300) has been considered in this analysis, corresponding to a PV module of 300 W_p with an area of 1.66 m^2, as in (Ilse et al., 2019b).

Table 8. Maximum allowed monitoring cost per sensor (in €/sensor) and confidence interval depending on the soiling rate reduction and the portion of mitigation costs spent for monitoring

	Assumed Soiling Rate Reduction			
	−20%		−50%	
	Portion of Mitigation Costs Spent for Monitoring			
PV Capacity	90.9%	9.09%	90.9%	9.09%
1–5 MW	4,668±1,764	528±178	13,613±4,587	1,375±463
5–40 MW	11,811±3,393	1,193±342	30,710±8,825	3,102±891
40–100 MW	44,506±4,243	4,495±428	115,718±11,034	11,688±1,114
>100 MW	407,929±330,498	41,205±33,383	1060,616±859,298	107,133±86,797

Data calculated from the maximum allowed mitigation costs reported in (Ilse et al., 2019b) and assuming a PV module efficiency of 18.1%, optimum cleaning cycles, power purchase prices of 0.03 €/kWh, a 10-year payback period, and a 5% discount rate.

As it can be seen in Table 8, the maximum allowed cost per sensor changes with the effectiveness of soiling mitigation and the size of the power plant. This represents the maximum investment that can be made to install and operate soiling monitors in each scenario and that would return a positive Net Present Value. For each scenario, the lower the actual cost compared with maximum allowed cost, the larger the NPV.

Because of the non-linearity between number of sensors and PV system size, larger plants will allow for more expensive and more accurate sensors, thanks to the lower number of sensors recommended per unit of capacity. On the other hand, smaller plants will necessarily require alternative, more economical solutions. In addition, the more the soiling loss is reduced (i.e. the more profits are made through soiling mitigation), the more capitals could ideally be placed into monitoring.

The analysis here presented is representative and does not take into account the variability of environmental and socio-economic conditions that affect the energy and economic impact of soiling. Indeed, the maximum allowed costs for soiling mitigation and soiling monitoring should be adapted to the specific conditions of each site. The analysis is based on the average soiling loss estimations presented by (Ilse et al., 2019b). However, the site-specific severity of the losses of a PV plant can also influence the profits of soiling mitigation. The higher the losses, the more the profits are ideally possible through soiling mitigation. Moreover, additional factors, such as degradation and electricity price, can impact the revenues of soiling mitigation (Micheli et al., 2020d) and therefore affect the capital available for soiling monitoring.

CONCLUSIONS

Soiling can be a severe issue for PV systems worldwide, becoming even more concerning because of the rapid PV market expansion. Mitigation strategies have to be put in place to eliminate or reduce its effects and have to be tailored to the specific conditions and configuration of each PV site. In addition, the intrinsic complexity and variability of soiling make it still difficult to predict. For these reasons, it has to be constantly monitored.

From the analysis of the size distribution of PV plants in five countries, it was possible to calculate the number of soiling sensors needed and to estimate the near future requirements by the fast growing PV market. In addition, a comprehensive analysis of the different soiling monitoring methodologies is presented, and the main challenges and perspectives of each strategy are discussed. Several soiling monitors are already commercially available, including novel low cost and low maintenance solutions. These are assessed, and future research and development directions are highlighted.

Soiling can also be estimated directly from PV performance data or from environmental parameters, without the need of installing specific soiling monitors. Models presented in the literature have been described, and the lack of and the consequent need for comparative studies have been emphasized.

Last, an economic analysis has been presented to estimate the maximum allowed monitoring cost, based on a previously presented assessment of soiling mitigation. The results show that the allowed expenditure for soiling monitoring varies depending on the system size and the effectiveness of the soiling mitigation strategy. In particular, the larger the PV system and the higher the soiling loss recovery after mitigation, the higher the maximum allowed cost for soiling monitoring and mitigation.

ACKNOWLEDGMENTS

Part of this work was funded through the European Union's Horizon 2020 research and innovation program under the NoSoilPV project (Marie Skłodowska-Curie grant agreement No. 793120). This job is part of ROM-PV project, supported under the umbrella of SOLAR-ERA.NET Cofund by the General Secretariat for Research and Technology (GSRT), the Ministry of Economy, Industry and Competitiveness – State Research Agency (MINECO-AEI) (IOM-PV, PCI2019-111852-2), and the Research and Innovation Foundation (RIF) of Cyprus. SOLAR-ERA.NET is supported by the European Commission within the EU Framework Program for Research and Innovation HORIZON 2020 (Cofund ERA-NET Action, N° 691664).

Figure 1 is reprinted with permission from Smestad et al. Creative Commons CC. The left picture in Figure 5 has been provided by Jesús Montes-Romero, University of Jaén (Spain), kindly acknowledged. The authors would like to thank Mark Korevaar, OTT HydroMet, and Bill Stueve, Atonometrics, for providing the left and right pictures of Figure 13, respectively.

AUTHOR CONTRIBUTIONS

Conceptualization: L.M. Methodology: J.G.B., L.M., E. F. F., and F. A. Investigation: J.G.B. and L.M. Formal Analysis: J.G.B. Visualization: J.G.B. and L.M. Data Curation: J.G.B. Validation: L.M. Writing—Original Draft: J.G.B. and L.M. Writing—Review & Editing: E. F. F. and F. A. Resources: E. F. F. and F. A. Supervision: L.M. and E.F.F.

DECLARATION OF INTERESTS

Dr. Leonardo Micheli, Dr. Eduardo F. Fernandez, and Prof. Florencia Almonacid declare an interest as co-inventors of a patented optical soiling detector.

REFERENCES

Al-Housani, M., Bicer, Y., and Koç, M. (2019). Experimental investigations on PV cleaning of large-scale solar power plants in desert climates: comparison of cleaning techniques for drone retrofitting. Energy Convers. Manag. *185*, 800–815.

AlDowsari, A., Bkayrat, R., AlZain, H., and Shahin, T. (2014). Best practices for mitigating soiling risk on PV POWER plants. In 2014 Saudi Arabia Smart Grid Conference SASG 2014 0–6. https://doi.org/10.1109/SASG.2014.7274291.

Alzubi, F.G., Alkandary, A., and Al-Asfour, A.T. (2018). Investigating the technical effectiveness of different photovoltaic cleaning methods in dust-intensive climates. In 35th European Photovoltaic Solar Energy Conference and Exhibition, pp. 1514–1518, https://doi.org/10.4229/35THEUPVSEC20182018-6BO.5.2.

Ångström, A. (1929). On the atmospheric transmission of sun radiation and on dust in the air. Geogr. Ann. *11*, 156–166.

Appels, R., Lefevre, B., Herteleer, B., Goverde, H., Beerten, A., Paesen, R., De Medts, K., Driesen, J., and Poortmans, J. (2013). Effect of soiling on photovoltaic modules. Sol. Energy *96*, 283–291.

Bahattab, M.A., Alhomoudi, I.A., Alhussaini, M.I., Mirza, M., Hegmann, J., Glaubitt, W., and Löbmann, P. (2016). Anti-soiling surfaces for PV applications prepared by sol-gel processing: comparison of laboratory testing and outdoor exposure. Sol. Energy Mater. Sol. Cells *157*, 422–428.

Bergin, M.H., Ghoroi, C., Dixit, D., Schauer, J.J., and Shindell, D.T. (2017). Large reductions in solar energy production due to dust and particulate air pollution. Environ. Sci. Technol. Lett. *4*, 339–344.

Bergin, M.H., Greenwald, R., Xu, J., Berta, Y., and Chameides, W.L. (2001). Influence of aerosol dry deposition on photosynthetically active radiation available to plants: a case study in the Yangtze delta region of China. Geophys. Res. Lett. *28*, 3605–3608.

Besson, P., Munoz, C., Ramirez-Sagner, G., Salgado, M., Escobar, R., and Platzer, W. (2017). Long-term soiling analysis for three photovoltaic technologies in Santiago region. IEEE J. Photovolt. *7*, 1755–1760.

Boyle, L., 2015. Don't soil your chances with solar Energy : experiments of natural dust accumulation on solar modules and the effect on light transmission by. Ph.D. thesis Submitt. to Fac. Grad. Sch. Univ. Color. https://scholar.colorado.edu/concern/graduate_thesis_or_dissertations/f1881m18s.

Boyle, L., Flinchpaugh, H., and Hannigan, M. (2016). Assessment of PM dry deposition on solar energy harvesting systems: measurement-model comparison. Aerosol Sci. Technol. *50*, 380–391.

Boyle, L., Flinchpaugh, H., and Hannigan, M. (2014). Ambient airborne particle concentration and soiling of PV cover plates. In 2014 IEEE 40th Photovoltaic Specialists Conference PVSC 2014, pp. 3171–3173, https://doi.org/10.1109/PVSC.2014.6925609.

Boyle, L., Flinchpaugh, H., and Hannigan, M. (2013). Impact of natural soiling on the transmission of PV cover plates. In Conference Record of IEEE Photovoltaic Specialists Conference, pp. 3276–3278, https://doi.org/10.1109/PVSC.2013.6745150.

Boyle, L., Flinchpaugh, H., and Hannigan, M.P. (2015). Natural soiling of photovoltaic cover plates and the impact on transmission. Renew. Energy *77*, 166–173.

Bundesnetzagentur. (2017). Pow-er plant list. https://www.bundesnetzagentur.de/EN/Areas/Energy/Companies/SecurityOfSupply/GeneratingCapacity/PowerPlantList/PubliPowerPlantList_node.html.

Burton, P.D., Boyle, L., Griego, J.J.M., and King, B.H. (2015). Quantification of a minimum detectable soiling level to affect photovoltaic devices by natural and simulated soils. IEEE J. Photovolt. *5*, 1143–1149.

Burton, P.D., Hendrickson, A., Ulibarri, S.S., Riley, D., Boyson, W.E., and King, B.H. (2016). Pattern effects of soil on photovoltaic surfaces. IEEE J. Photovolt. *6*, 976–980.

Cabanillas, R.E., and Munguía, H. (2011). Dust accumulation effect on efficiency of Si photovoltaic modules. J. Renew. Sustain. Energy *3*, 1–10.

Cano, J., John, J.J., Tatapudi, S., and Tamizhmani, G. (2014). Effect of tilt angle on soiling of photovoltaic modules. In 2014 IEEE 40th Photovoltaic Specialists Conference PVSC 2014, pp. 3174–3176, https://doi.org/10.1109/PVSC.2014.6925610.

Caron, J.R., and Littmann, B. (2013). Direct monitoring of energy lost due to soiling on first solar modules in California. IEEE J. Photovolt. *3*, 336–340.

Coello, M., and Boyle, L. (2019). Simple model for predicting time series soiling of photovoltaic panels. IEEE J. Photovolt. *9*, 1382–1387.

Conceição, R., Merrouni, A.A., Lopes, D., Alae, A., Silva, H.G., Bennouna, E.G., Collares-Pereira, M., and Ghennioui, A. (2019a). A comparative study of soiling on solar mirrors in Portugal and Morocco: preliminary results for the dry season. In AIP Conference Proceedings, *2126*AIP Conference Proceedings. https://doi.org/10.1063/1.5117760.

Conceição, R., Silva, H.G., Fialho, L., Lopes, F.M., and Collares-Pereira, M. (2019b). PV system design with the effect of soiling on the optimum tilt angle. Renew. Energy *133*, 787–796.

Conceição, R., Silva, H.G., Mirão, J., and Collares-Pereira, M. (2018a). Organic soiling: the role of pollen in PV module performance degradation. Energies *11*, 1–13.

Conceição, R., Silva, H.G., Mirão, J., Gostein, M., Fialho, L., Narvarte, L., and Collares-Pereira, M. (2018b). Saharan dust transport to Europe and its impact on photovoltaic performance: a case study of soiling in Portugal. Sol. Energy *160*, 94–102.

Conceição, R., Vázquez, I., Fialho, L., and García, D. (2020). Soiling and rainfall effect on PV technology in rural Southern Europe. Renew. Energy *156*, 743–747.

Consejería de Medio Ambiente (2020). Informes de calidad de aire. http://www.juntadeandalucia.es/medioambiente/site/rediam/menuitem.04dc44281e5d53cf8ca78ca731525ea0/?vgnextoid=7e612e07c3dc4010VgnVCM1000000624e50aRCRD&vgnextchannel=762e90a63670f210VgnVCM2000000624e50aRCRD&vgnextfmt=rediam&lr=lang_es.

Cordero, R.R., Damiani, A., Laroze, D., MacDonell, S., Jorquera, J., Sepúlveda, E., Feron, S., Llanillo, P., Labbe, F., Carrasco, J., et al. (2018). Effects of soiling on photovoltaic (PV) modules in the Atacama Desert. Sci. Rep. *8*, 1–14.

Costa, S.C.S., Diniz, A.S.A.C., Duarte, T., Bhaduri, S., Santana, V.C., and Kazmerski, L.L. (2019). Performance of soiled PV module technologies: behavior based on controverted parameters. In Conference Record of the Twenty Sixth IEEE Photovoltaic Specialists Conference, *540*Conference Record of the Twenty Sixth IEEE Photovoltaic Specialists Conference, pp. 1–5, https://doi.org/10.1109/PVSC40753.2019.8980675.

Costa, S.C.S., Diniz, A.S.A.C., and Kazmerski, L.L. (2018). Solar energy dust and soiling R&D progress: literature review update for 2016. Renew. Sustain. Energy Rev. *82*, 2504–2536.

Costa, S.C.S., Diniz, A.S.A.C., and Kazmerski, L.L. (2016). Dust and soiling issues and impacts relating to solar energy systems: literature review update for 2012-2015. Renew. Sustain. Energy Rev. *63*, 33–61.

Csavina, J., Field, J., Félix, O., Corral-Avitia, A.Y., Sáez, A.E., and Betterton, E.A. (2014). Effect of wind speed and relative humidity on atmospheric dust concentrations in semi-arid climates. Sci. Total Environ. *487*, 82–90.

Curtis, T., Tatapudi, S., and Tamizh Mani, G.S. (2018). Design and operation of a waterless pv soiling monitoring station. In 2018 IEEE 7th World Conference on Photovoltaic Energy Conversion, WCPEC 2018 - a Joint Conference of 45th IEEE PVSC, 28th PVSEC 34th EU PVSEC, pp. 3407–3412, https://doi.org/10.1109/PVSC.2018.8547820.

Deceglie, M.G., Micheli, L., and Muller, M. (2018a). Quantifying soiling loss directly from PV yield. IEEE J. Photovolt. *8*, 547–551.

Deceglie, M.G., Micheli, L., and Muller, M. (2017). Quantifying year-to-year variations in solar panel soiling from PV energy-production data. In 2017 IEEE 44th Photovoltaic Specialists Conference PVSC 2017, pp. 1–6, https://doi.org/10.1109/PVSC.2017.8366290.

Deceglie, M.G., Muller, M., Defreitas, Z., and Kurtz, S. (2018b). A scalable method for extracting soiling rates from PV production data. In 2017 IEEE 44th Photovoltaic Specialists Conference PVSC 2017, pp. 1–5, https://doi.org/10.1109/PVSC.2017.8366465.

Deceglie, M.G., Muller, M., Jordan, Di.C., and Deline, C. (2019). Numerical validation of an algorithm for combined soiling and degradation analysis of photovoltaic systems. In Conference Record of the IEEE Photovoltaic Specialists Conference, pp. 3111–3114, https://doi.org/10.1109/PVSC40753.2019.8981183.

Defreitas, Z., Ramirez, A., Huang, B., Kurtz, S., Muller, M., and Deceglie, M. (2019). Evaluating the accuracy of various irradiance models in detecting soiling of irradiance sensors. In Conference Record of the IEEE Photovoltaic Specialists Conference, pp. 2223–2228, https://doi.org/10.1109/PVSC40753.2019.8981194.

Duarte, T.P., Diniz, A.S.A.C., Costa, S.C.S., and Lawrence. (2020). PV module technology Comparisons : comprehensive study differentiating soiling spectral effects , operating temperature , and climate conditions. In IEEE 47th Photovoltaic Specialist Conference (PVSC). Virtual.

Einhorn, A., Micheli, L., Miller, D.C., Simpson, L.J., Moutinho, H.R., To, B., Lanaghan, C.L., Muller, M.T., Toth, S., John, J.J., et al. (2019). Evaluation of soiling and potential mitigation approaches on photovoltaic glass. IEEE J. Photovolt. *9*, 233–239.

El-Nashar, A.M. (2003). Effect of dust deposition on the performance of a solar desalination plant operating in an arid desert area. Sol. Energy *75*, 421–431.

Electra Spain (2019). Conjunto de datos de productores de energia electrica. https://sedeaplicaciones.minetur.gob.es/electra/BuscarDatos.aspx.

Elminir, H.K., Ghitas, A.E., Hamid, R.H., El-Hussainy, F., Beheary, M.M., and Abdel-Moneim, K.M. (2006). Effect of dust on the transparent cover of solar collectors. Energy Convers. Manag. *47*, 3192–3203.

Energy Services Manager GSE SpA (2019). Atlasoe Italy. http://atlasole.gse.it/atlasole/.

Etyemezian, V., Nikolich, G., and Gillies, J.A. (2017). Mean flow through utility scale solar facilities and preliminary insights on dust impacts. J. Wind Eng. Ind. Aerodyn. *162*, 45–56.

Fathi, M., Abderrezek, M., and Grana, P. (2017). Technical and economic assessment of cleaning protocol for photovoltaic power plants: case of Algerian Sahara sites. Sol. Energy *147*, 358–367.

Federal Ministry for Economic Affairs and Energy (2017). Renewable energy sources act Dz. U *201*, 1–221.

Fernández, E.F., Ferrer-Rodríguez, J.P., Almonacid, F., and Pérez-Higueras, P. (2017). Current-voltage dynamics of multi-junction CPV modules under different irradiance levels. Sol. Energy *155*, 39–50.

Figgis, B., Ennaoui, A., Ahzi, S., and Remond, Y. (2016a). Review of PV soiling measurement methods. In Proc. 2016 Int. Renew. Sustain. Energy Conf. IRSEC 2016, pp. 176–180, https://doi.org/10.1109/IRSEC.2016.7984027.

Figgis, B., Ennaoui, A., Ahzi, S., and Rémond, Y. (2017). Review of PV soiling particle mechanics in desert environments. Renew. Sustain. Energy Rev. *76*, 872–881.

Figgis, B., Ennaoui, A., Guo, B., Javed, W., and Chen, E. (2016b). Outdoor soiling microscope for measuring particle deposition and resuspension. Sol. Energy *137*, 158–164.

Figgis, B., Goossens, D., Guo, B., and Ilse, K. (2019). Effect of tilt angle on soiling in perpendicular wind. Sol. Energy *194*, 294–301.

Figgis, B., Guo, B., Javed, W., Ahzi, S., and Rémond, Y. (2018). Dominant environmental parameters for dust deposition and resuspension in desert climates. Aerosol Sci. Technol. *52*, 788–798.

García, M., Marroyo, L., Lorenzo, E., and Pérez, M. (2011). Soiling and other optical losses in solar-tracking PV plants in navarra. Prog. Photovolt. Res. Appl. *19*, 211–217.

Gostein, M., Bourne, B., Farina, F., Flottemesch, R., Giosa, E., Kagan, S., Stueve, B., and Zureick, F. (2019). Field evaluations of Mars ™ optical soiling sensor. IEEE 46th Photovoltaic Specialist Conference (PVSC).

Gostein, M., Bourne, B., Farina, F., and Stueve, B. (2020). Field testing of Mars ™ soiling sensor. In

IEEE 47th Photovoltaic Specialist Conference (PVSC). Virtual.

Gostein, M., Caron, J.R., and Littmann, B. (2014). Measuring soiling losses at utility-scale PV power plants. In 2014 IEEE 40th Photovoltaic Specialists Conference PVSC, pp. 2014 885–890, https://doi.org/10.1109/PVSC.2014.6925056.

Gostein, M., Duster, T., and Thuman, C. (2015). Accurately measuring PV soiling losses with soiling station employing module power measurements. In 2015 IEEE 42nd Photovoltaic Specialists Conference PVSC 2015. https://doi.org/10.1109/PVSC.2015.7355993.

Gostein, M., Faullin, S., Miller, K., Schneider, J., and Stueve, B. (2018a). Mars soiling Sensor^{TM}. In 2018 IEEE 7th World Conference on Photovoltaic Energy Conversion, WCPEC 2018 - a Joint Conference of 45th IEEE PVSC, 28th PVSEC 34th EU PVSEC, pp. 3417–3420, https://doi.org/10.1109/PVSC.2018.8547767.

Gostein, M., Littmann, B., Caron, J.R., and Dunn, L. (2013). Comparing PV power plant soiling measurements extracted from PV module irradiance and power measurements. In Conference Record of IEEE Photovoltaic Specialists Conference, pp. 3004–3009, https://doi.org/10.1109/PVSC.2013.6745094.

Gostein, M., Passow, K., Deceglie, M.G., Micheli, L., and Stueve, B. (2018b). Local variability in PV soiling rate. In 2018 IEEE 7th World Conference on Photovoltaic Energy Conversion, WCPEC 2018 - a Joint Conference of 45th IEEE PVSC, 28th PVSEC 34th EU PVSEC, pp. 3421–3425, https://doi.org/10.1109/PVSC.2018.8548049.

Government of India (2019). Ministry of new and renewable energy. https://mnre.gov.in/.

Guo, B., Javed, W., Figgis, B.W., and Mirza, T. (2015). Effect of dust and weather conditions on photovoltaic performance in Doha, Qatar. In 2015 1st Workshop on Smart Grid and Renewable Energy, SGRE 2015, pp. 1–6, https://doi.org/10.1109/SGRE.2015.7208718.

Gupta, V., Sharma, M., Pachauri, R.K., and Dinesh Babu, K.N. (2019). Comprehensive review on effect of dust on solar photovoltaic system and mitigation techniques. Sol. Energy *191*, 596–622.

Hammond, R., Srinivasan, D., Harris, A., Whitfield, K., and Wohlgemuth, J. (1997). Effects of soiling on PV module and radiometer performance. In Conference Record of the IEEE Photovoltaic Specialists Conference, pp. 1121–1124, https://doi.org/10.1109/pvsc.1997.654285.

Hegazy, A.a (2001). Effect of dust accumulation on solar transmittance through glass covers of plate-type collectors. Renew. Energy *22*, 525–540.

Herrmann, J., Slamova, K., Glaser, R., and Köhl, M. (2014). Modeling the soiling of glazing materials in arid regions with geographic information systems (GIS). Energy Proced. *48*, 715–720.

Ilse, K., Figgis, B., Khan, M.Z., Naumann, V., and Hagendorf, C. (2019a). Dew as a detrimental influencing factor for soiling of PV modules. IEEE J. Photovoltaics *9*, 287–294.

Ilse, K., Micheli, L., Figgis, B.W., Lange, K., Daßler, D., Hanifi, H., Wolfertstetter, F., Naumann, V., Hagendorf, C., and Gottschalg, R. (2019b). Techno-Economic Assessment of Soiling Losses and Mitigation Strategies for Solar Power Generation 1–19. https://doi.org/10.1016/j.joule.2019.08.019.

Ilse, K.K., Figgis, B.W., Naumann, V., Hagendorf, C., and Bagdahn, J. (2018). Fundamentals of soiling processes on photovoltaic modules. Renew. Sustain. Energy Rev. *98*, 239–254.

Instituto Nacional de Estadística (2019). Población del Padrón Continuo por Unidad Poblacional. https://www.ine.es/nomen2/index.do?accion=busquedaAvanzada&entidad_amb=no&codProv=23&codMuni=50&codEC=0&codES=0&codNUC=0&denominacion_op=like&denominacion_txt=&L=0.

International Electrotechnical Commission, 2017. Photovoltaic System Performance – Part 1: Monitoring (IEC 61724-1, Edition 1.0, 2017-03). CENELEC.

Isaifan, R.J., Johnson, D., Ackermann, L., Figgis, B., and Ayoub, M. (2019). Evaluation of the adhesion forces between dust particles and photovoltaic module surfaces. Sol. Energy Mater. Sol. Cells *191*, 413–421.

Jahn, U., Herz, M., and Rheinland, T. (2018). Review on Infrared (IR) and Electroluminescence (EL) Imaging for Photovoltaic Field Applications (IEA-Photovoltaic Power Systems Programme).

Jamil, W.J., Abdul Rahman, H., Shaari, S., and Salam, Z. (2017). Performance degradation of photovoltaic power system: review on mitigation methods. Renew. Sustain. Energy Rev. *67*, 876–891.

Javed, W., Guo, B., and Figgis, B. (2017a). Modeling of photovoltaic soiling loss as a function of environmental variables. Sol. Energy *157*, 397–407.

Javed, W., Guo, B., Figgis, B., Martin Pomares, L., and Aïssa, B. (2020). Multi-year field assessment of seasonal variability of photovoltaic soiling and environmental factors in a desert environment. Sol. Energy *211*, 1392–1402.

Javed, W., Wubulikasimu, Y., Figgis, B., and Guo, B. (2017b). Characterization of dust accumulated on photovoltaic panels in Doha. Qatar. Sol. Energy *142*, 123–135.

Jiang, H., Lu, L., and Sun, K. (2011). Experimental investigation of the impact of airborne dust deposition on the performance of solar photovoltaic (PV) modules. Atmos. Environ. *45*, 4299–4304.

Jiménez-Torres, M., Rus-Casas, C., Lemus-Zúñiga, L.G., and Hontoria, L. (2017). The importance of accurate solar data for designing solar photovoltaic systems-Case studies in Spain. Sustainability *9*, https://doi.org/10.3390/su9020247.

John, J.J., Rajasekar, V., Boppana, S., Chattopadhyay, S., and Kottantharayil, A. (2015). Quantification and modeling of spectral and angular losses of naturally soiled PV modules. IEEE J. Photovolt. *5*, 1727–1734.

John, J.J., Warade, S., Tamizhmani, G., and Kottantharayil, A. (2016). Study of soiling loss on photovoltaic modules with artificially deposited dust of different gravimetric densities and compositions collected from different locations in India. IEEE J. Photovolt. *6*, 236–243.

Jones, R.K., Baras, A., Saeeri, A.A., Al Qahtani, A., Al Amoudi, A.O., Al Shaya, Y., Alodan, M., and Al-Hsaien, S.A. (2016). Optimized cleaning cost and schedule based on observed soiling conditions for photovoltaic plants in Central Saudi Arabia. IEEE J. Photovolt. https://doi.org/10.1109/JPHOTOV.2016.2535308.

Kaldellis, J.K., and Kapsali, M. (2011). Simulating the dust effect on the energy performance of photovoltaic generators based on experimental measurements. Energy *36*, 5154–5161.

Kalogirou, S.A., Agathokleous, R., and Panayiotou, G. (2013). On-site PV characterization and the effect of soiling on their performance. Energy *51*, 439–446.

Karim, M., Delord, C., Raccurt, O., and Naamane, S. (2018). Exposure conditions effect on soiling of solar glass mirrors. In AIP Conference Proceedings 2033. https://doi.org/10.1063/1.5067234.

Kazem, A.A., Chaichan, M.T., and Kazem, H.A. (2014). Dust effect on photovoltaic utilization in Iraq: review article. Renew. Sustain. Energy Rev. *37*, 734–749.

Kazmerski, L.L., Diniz, A.S.A.C., Braga, D.S., Maia, C.B., Viana, M.M., Costa, S.C., Brito, P.P., Campos, C.D., de Morais Hanriot, S., and de Oliveira Cruz, L.R. (2018). Interrelationships Among Non-uniform Soiling Distributions and PV Module Performance Parameters, Climate Conditions, and Soiling Particle and Module Surface Properties 2307–2311. https://doi.org/10.1109/pvsc.2017.8366584.

Kim, Y., Wellum, G., Mello, K., Strawhecker, K.E., Thoms, R., Giaya, A., and Wyslouzil, B.E. (2016). Effects of relative humidity and particle and surface properties on particle resuspension rates. Aerosol Sci. Technol. *50*, 339–352, https://doi.org/10.1080/02786826.2016.1152350.

Kimber, A., Mitchell, L., Nogradi, S., and Wenger, H. (2007). The effect of soiling on large grid-connected photovoltaic systems in California and the Southwest Region of the United States. In Conference Record of 2006 IEEE 4th World Conference on Photovoltaic Energy Conversion WCPEC-4 2, pp. 2391–2395, https://doi.org/10.1109/WCPEC.2006.279690.

King, D.L., Boyson, W.E., and Kratochvill, J.A. (2004). Photovoltaic Array Performance Model. https://doi.org/10.2172/919131.

Korevaar, M., Bergmans, T., Mes, J., Mechelen, X.van, Merrouni, A.A., Wolfertstetter, F., and Wilbert, S. (2019). Field tests of soiling detection system for PV modules. In 36th EU PVSEC.

Korevaar, M., Mes, J., Nepal, P., Snijders, G., and van, M.X. (2017). Novel soiling detection system for solar panels. In 33rd European Photovoltaic Solar Energy Conference and Exhibition. https://doi.org/10.4229/EUPVSEC20172017-6BV.2.11.

Korevaar, M., van Mechelen, X., Nepal, P., Bergmans, T., Alami Merrouni, A., and Mes, J. (2018). Unique soiling detection system for PV modules. In European Photovoltaic Solar. Energy Conference and. Exhibition, pp. 1988–1990, https://doi.org/10.4229/35THEUPVSEC20182018-6DV.1.8.

Kottek, M., Grieser, J., Beck, C., Rudolf, B., and Rubel, F. (2006). World map of the Köppen-Geiger climate classification updated. Meteorol. Z. *15*, 259–263.

Laarabi, B., El Baqqal, Y., Dahrouch, A., and Barhdadi, A. (2020). Deep analysis of soiling effect on glass transmittance of PV modules in seven sites in Morocco. Energy *213*, 118811.

Labbe, R.R. (2016). Kalman and Bayesian Filters in Python. https://elec3004.uqcloud.net/2015/tutes/Kalman_and_Bayesian_Filters_in_Python.pdf.

Li, J., Carlson, B.E., and Lacis, A.A. (2015). How well do satellite AOD observations represent the spatial and temporal variability of PM2.5 concentration for the United States? Atmos. Environ. *102*, 260–273.

Li, X., Mauzerall, D.L., and Bergin, M.H. (2020). Global reduction of solar power generation efficiency due to aerosols and panel soiling. Nat. Sustain. https://doi.org/10.1038/s41893-020-0553-2.

Lorenzo, E., Moretón, R., and Luque, I. (2014). Dust effects on PV array performance: in-field observations with non-uniform patterns. Prog. Photovolt. Res. Appl. *22*, 666–670.

Madeti, S.R., and Singh, S.N. (2017). Monitoring system for photovoltaic plants: a review. Renew. Sustain. Energy Rev. *67*, 1180–1207.

Mani, F., Pulipaka, S., and Kumar, R. (2016). Characterization of power losses of a soiled PV panel in Shekhawati region of India. Sol. Energy *131*, 96–106.

Massi Pavan, A., Mellit, A., and De Pieri, D. (2011). The effect of soiling on energy production for large-scale photovoltaic plants. Sol. Energy *85*, 1128–1136.

Mehta, S., Azad, A.P., Chemmengath, S.A., Raykar, V., and Kalyanaraman, S. (2018). DeepSolarEye: power loss prediction and Weakly supervised soiling Localization via fully convolutional networks for solar panels. In Proceedings - 2018 IEEE Winter Conference on Applications of Computer Vision, WACV 2018 2018-January, pp. 333–342, https://doi.org/10.1109/WACV.2018.00043.

Mejia, F., Kleissl, J., and Bosch, J.L. (2014). The effect of dust on solar photovoltaic systems. Energy Proced. *49*, 2370–2376.

Mejia, F.A., and Kleissl, J. (2013). Soiling losses for solar photovoltaic systems in California. Sol. Energy *95*, 357–363.

Micheli, L., and Deceglie, M.G. (2018). Predicting future soiling losses using environmental data. In European Photovoltaic Solar. Energy Conference and. Exhibition, pp. 1–4.

Micheli, L., Deceglie, M.G., and Muller, M. (2019a). Mapping photovoltaic soiling using spatial interpolation techniques. IEEE J. Photovolt. *9*, 272–277.

Micheli, L., Deceglie, M.G., and Muller, M. (2019b). Predicting photovoltaic soiling losses using environmental parameters: an update. Prog. Photovolt. Res. Appl. *27*, 210–219.

Micheli, L., Fernández, E.F., Aguilera, J.T., and Almonacid, F. (2021). Economics of seasonal photovoltaic soiling and cleaning optimization scenarios. Energy *215*, 119018.

Micheli, L., Fernandez, E.F., Caballero, J.A., Smestad, G.P., Nofuentes, G., Mallick, T.K., and Almonacid, F. (2019c). Correlating Photovoltaic Soiling Losses to Waveband and Single-Value Transmittance Measurements. Energy *180*, 376–386.

Micheli, L., Fernandez, E.F., Muller, M., and Almonacid, F. (2020a). Extracting and generating PV soiling profiles for analysis, forecasting, and cleaning optimization. IEEE J. Photovolt. *10*, 197–205.

Micheli, L., Fernández, E.F., Muller, M., Smestad, G.P., and Almonacid, F. (2020b). Selection of optimal wavelengths for optical soiling modelling and detection in photovoltaic modules. Sol. Energy Mater. Sol. Cells *212*, https://doi.org/10.1016/j.solmat.2020.110539.

Micheli, L., Fernández, E.F., Smestad, G.P., Alrashidi, H., Sarmah, N., Hassan, I.A.I., Kasry, A., Nofuentes, G., Sood, N., Pesala, B., et al. (2017a). A unified global investigation on the spectral effects of soiling losses of PV glass substrates: preliminary results. In 43rd IEEE Photovoltaic Specialists Conference, pp. 3–8.

Micheli, L., and Muller, M. (2017). An investigation of the key parameters for predicting PV soiling losses. Prog. Photovolt. Res. Appl. https://doi.org/10.1002/pip.2860.

Micheli, L., Muller, M., Fernandez, E.F., Fernández, E.F., and Almonacid, F.M. (2020c). Segmentation of deposition periods: an opportunity to improve PV soiling extractio. In IEEE 45th Photovoltaic Specialist Conference (PVSC).

Micheli, L., Muller, M., and Kurtz, S. (2016). Determining the effects of environment and atmospheric parameters on PV field performance. In 2016 IEEE 43rd Photovoltaic Specialist Conference (PVSC) (IEEE), pp. 1724–1729, https://doi.org/10.1109/PVSC.2016.7749919.

Micheli, L., Ruth, D., and Muller, M. (2017b). Seasonal trends of soiling on photovoltaic systems. In 2017 IEEE 44th Photovoltaic Specialist Conference (PVSC) (IEEE). https://doi.org/10.1109/PVSC.2017.8366381.

Micheli, L., Theristis, M., Talavera, D.L., Almonacid, F., Stein, J.S., and Fernandez, E.F. (2020d). Photovoltaic cleaning frequency optimization under different degradation rate patterns. Renew. Energy. https://doi.org/10.1016/j.renene.2020.11.044.

Mondal, S., Mondal, A.K., Sharma, A., Devalla, V., Rana, S., Kumar, S., and Pandey, J.K. (2018). An overview of cleaning and prevention processes for enhancing efficiency of solar photovoltaic panels. Curr. Sci. *115*, 1065–1077.

Morley, K., Robinson, J., Chard, J., and Peterson, J. (2020). In-situ comparison of five soiling measurement systems. In PVPMC Webinar on Solar Resource Assessment.

Muller, M., Micheli, L., and Martinez-Morales, A.A. (2018a). A Method to Extract Soiling Loss Data from Soiling Stations with Imperfect Cleaning Schedules 2881–2886. https://doi.org/10.1109/pvsc.2017.8366214.

Muller, M., Morse, J., Micheli, L., Almonacid, F., Fernandez, E.F., 2018b. Design and Indoor Validation of "DUSST": A Novel Low-Maintenance Soiling Station. 35th European Photovoltaic Solar Energy Conference and Exhibition 1991-1995.

Naeem, M., and Tamizhmani, G. (2016). Climatological Relevance to the Soiling Loss of Photovoltaic Modules. In 2015 Saudi Arabia Smart Grid, SASG 2015, pp. 1–5, https://doi.org/10.1109/SASG.2015.7449280.

Nahar, N.M., and Gupta, J.P. (1990). Effect of dust on transmittance of glazing materials for solar collectors under arid zone conditions of India. Sol. Wind Technol. *7*, 237–243.

National Renewable Energy Laboratory, 2018a. Photovoltaic Modules Soiling Map. https://www.nrel.gov/pv/soiling.html.

National Renewable Energy Laboratory, 2018b. PV_soiling: Code for Extracting Soiling Loss from PV Plant Data. https://github.com/NREL/pv_soiling.

Naumann, V., Hagendorf, C., Bagdahn, J., Werner, M., Pöllmann, H., Figgis, B.W., and Ilse, K.K. (2018). Comprehensive analysis of soiling and cementation processes on PV modules in Qatar. Sol. Energy Mater. Sol. Cells *186*, 309–323.

Nayshevsky, I., Xu, Q., and Lyons, A.M. (2019). Hydrophobic-hydrophilic surfaces exhibiting dropwise condensation for anti-soiling applications. IEEE J. Photovolt. *9*, 302–307.

Nayshevsky, I., Xu, Q., Newkirk, J.M., Furhang, D., Miller, D.C., and Lyons, A.M. (2020). Self-cleaning hybrid hydrophobic-hydrophilic surfaces: durability and effect of artificial soilant particle type. IEEE J. Photovolt. *10*, 577–584.

Nofuentes, G., Gueymard, C.A., Aguilera, J., Pérez-Godoy, M.D., and Charte, F. (2017). Is the average photon energy a unique characteristic of the spectral distribution of global irradiance? Sol. Energy *149*, 32–43.

Numerical Optimization (2006). Numerical Optimization (Springer). https://doi.org/10.1007/978-0-387-40065-5.

OMIE, 2020. Evolucion del mercado de electricidad: Informe mensual Junio 2020. https://www.omie.es/es.

Pacini, E. (2015). Pollination. In Reference Module in Earth Systems and Environmental Sciences. https://doi.org/10.1016/b978-0-12-409548-9.09315-5.

Pelland, S., Pawar, P., Veeramani, A., Gustafson, W., and Etringer, L.L.A. (2018). Testing global models of photovoltaic soiling ratios against field test data worldwide. In 2018 IEEE 7th World Conference on Photovoltaic Energy Conversion,

WCPEC 2018 - a Joint Conference of 45th IEEE PVSC, 28th PVSEC 34th EU PVSEC, pp. 3442–3446, https://doi.org/10.1109/PVSC.2018.8548204.

Qasem, H., Betts, T.R., Müllejans, H., Albusairi, H., and Gottschalg, R. (2014). Dust-induced shading on photovoltaic modules. Prog. Photovolt. Res. Appl. https://doi.org/10.1002/pip.2230.

Qasem, H., Mnatsakanyan, A., and Banda, P. (2017). Assessing dust on PV modules using image processing techniques. In 2017 IEEE 44th Photovoltaic Specialists Conference PVSC 2017, 9712017 IEEE 44th Photovoltaic Specialists Conference PVSC 2017, pp. 1–5, https://doi.org/10.1109/PVSC.2017.8366466.

Rodrigo, P.M., Gutierrez, S., Micheli, L., Fernández, E.F., and Almonacid, F. (2020). Optimum cleaning schedule of photovoltaic systems based on levelised cost of energy and case study in central Mexico. Sol. Energy *209*, 11–20.

Roslizar, A., Dottermusch, S., Schmager, R., Guttmann, M., Gomard, G., Hölscher, H., Richards, B.S., and Paetzold, U.W. (2020). Hot-embossed microcone-textured fluoropolymer as self-cleaning and anti-reflective photovoltaic module covers. Sol. Energy Mater. Sol. Cells *214*, https://doi.org/10.1016/j.solmat.2020.110582.

Sanz Saiz, C., Polo Martínez, J., and Martín Chivelet, N. (2020). Influence of pollen on solar photovoltaic energy: literature review and experimental testing with pollen. Appl. Sci. *10*, 4733.

Sarver, T., Al-Qaraghuli, A., and Kazmerski, L.L. (2013). A comprehensive review of the impact of dust on the use of solar energy: History, investigations, results, literature, and mitigation approaches. Renew. Sustain. Energy Rev. *22*, 698–733.

Sayyah, A., Horenstein, M.N., and Mazumder, M.K. (2014). Energy yield loss caused by dust deposition on photovoltaic panels. Sol. Energy *107*, 576–604.

Schill, C., Brachmann, S., Heck, M., Weiss, K.-A., and Koehl, M. (2011). Impact of heavy soiling on the power output of PV-modules christian. SPIE Sol. Energy + Technol. *8112*, 811207–6.

Schill, C., Brachmann, S., and Koehl, M. (2015). Impact of soiling on IV-curves and efficiency of PV-modules. Sol. Energy *112*, 259–262.

Sehmel, G.A., and Sutter, S.L. (1974). Particle deposition rates on a water surface as a function of particle diameter and air velocity. J. Rech. Atmos. *8*, 911–920.

Shirakawa, M.A., Zilles, R., Mocelin, A., Gaylarde, C.C., Gorbushina, A., Heidrich, G., Giudice, M.C., Del Negro, G.M.B., and John, V.M. (2015). Microbial colonization affects the efficiency of photovoltaic panels in a tropical environment. J. Environ. Manage. *157*, 160–167.

Shrestha, S., and Taylor, M. (2016). Soiling assessment in large-scale PV arrays. Solarpro Mag. http://solarprofessional.com/articles/operations-maintenance/soiling-assessment-in-large-scale-pv-arrays?v=disable_pagination.

Skomedal, A., and Deceglie, M.G. (2020). Combined estimation of degradation and soiling losses in photovoltaic systems. IEEE J. Photovolt. *10*, 1788–1796.

Skomedal, Å., Haug, H., and Marstein, E.S. (2019). Endogenous soiling rate determination and detection of cleaning events in utility-scale PV plants. IEEE J. Photovolt. *9*, 858–863.

Smestad, G.P., Germer, T.A., Alrashidi, H., Fernández, E.F., Dey, S., Brahma, H., Sarmah, N., Ghosh, A., Sellami, N., Hassan, I.A.I., et al. (2020). Modelling photovoltaic soiling losses through optical characterization. Sci. Rep. *10*, 1–13.

Solar Power Europe (2020). Global market Outlook for solar power: 2020-2024. Glob. Mark. Outlook, 1–116.

Solar Power Europe (2019). Global market Outlook for solar power: 2019-2023. Glob. Mark. Outlook *92*, 1–92.

Solas, A.F., Micheli, L., Muller, M., Almonacid, F., and Fernández, E.F. (2020). Design, characterization and indoor validation of the optical soiling detector "DUSST". Sol. Energy *211*, 1459–1468.

Steinfeld, J.I., and Pandis, S.N. (1998). Atmospheric Chemistry and Physics: From Air Pollution to Climate Change. Environment: Science and Policy for Sustainable Development *40*, 26.

Stridh, B. (2012). Evaluation of economical benefit of cleaning of soiling and snow in PV plants at three European locations. In Conference Record of IEEE Photovoltaic Specialists Conference, pp. 1448–1451, https://doi.org/10.1109/PVSC.2012.6317869.

Supe, H., Avtar, R., Singh, D., Gupta, A., Yunus, A.P., Dou, J., Ravankar, A.A., Mohan, G., Chapagain, S.K., Sharma, V., et al. (2020). Google earth engine for the detection of soiling on photovoltaic solar panels in arid environments. Remote Sens. *12*, https://doi.org/10.3390/RS12091466.

Tamizhmani, G., King, B., Venkatesan, A., Deline, C., Pavgi, A., Tatapudi, S., Kuitche, J., Chokor, A., and Asmar, M. El (2016). Regional soiling stations for PV: soling loss analysis. In 2016 IEEE 43rd Photovoltaic Specialist Conference (PVSC), pp. 1741–1746, https://doi.org/10.1109/PVSC.2016.7749922.

Theristis, M., Livera, A., Jones, C.B., Makrides, G., Georghiou, G.E., and Stein, J. (2020). Nonlinear photovoltaic degradation rates: modeling and comparison against conventional methods. IEEE J. Photovolt. *10* (4), 1112–1118.

Toth, S., Hannigan, M., Vance, M., and Deceglie, M. (2020). Predicting photovoltaic soiling from air quality measurements. IEEE J. Photovolt *10* (4), 1142–1147.

Toth, S., Muller, M., Miller, D.C., Moutinho, H., To, B., Micheli, L., Linger, J., Engtrakul, C., Einhorn, A., and Simpson, L. (2018). Soiling and cleaning: initial observations from 5-year photovoltaic glass coating durability study. Sol. Energy Mater. Sol. Cells *185*, 375–384.

U.S. Energy Information Administration (2019). Capacity of Electric power plants. https://www.eia.gov/electricity/data.php.

Valerino, M., Bergin, M., Ghoroi, C., Ratnaparkhi, A., and Smestad, G.P. (2020). Low-cost solar PV soiling sensor validation and size resolved soiling impacts: a comprehensive field study in Western India. Sol. Energy *204*, 307–315.

Van Donkelaar, A., Martin, R.V., Brauer, M., Hsu, N.C., Kahn, R.A., Levy, R.C., Lyapustin, A., Sayer, A.M., and Winker, D.M. (2016). Global estimates of fine particulate matter using a combined geophysical-statistical method with information from satellites, models, and monitors. Environ. Sci. Technol. *50*, 3762–3772.

Wagner, F., and Vogel, B. (2019). Soiling of solar panels within PerduS project. In 6th Interenational Conference Energy Meteorology..

Walsh, R.P.D., and Lawler, D.M. (1981). Rainfall seasonality: description, spatial patterns and change through time. Weather *36*, 201–208.

Weber, B., Quiñones, A., Almanza, R., and Duran, M.D. (2014). Performance reduction of PV systems by dust deposition. Energy Proced. *57*, 99–108.

Yang, M., Ji, J., and Guo, B. (2020a). An image-based method for soiling quantification. In 2020 IEEE International Conference on Informatics, IoT, Enabling Technology. ICIoT 2020 89–94. https://doi.org/10.1109/ICIoT48696.2020.9089619.

Yang, M., Ji, J., Member, S., and Guo, B. (2020b). Soiling quantification uzsing an image-based Method : effects of imaging conditions. IEEE J. Photovolt. 1–8, https://doi.org/10.1109/JPHOTOV.2020.3018257.

Yap, W.K., Galet, R., and Yeo, K.C. (2015). Quantitative analysis of dust and soiling on solar pv panels in the tropics utilizing image-processing methods. In 2015 Asia-Pacific Sol. Res. Conf, 978-0-646-95016-7.

Yilbas, B.S., Ali, H., Khaled, M.M., Al-Aqeeli, N., Abu-Dheir, N., and Varanasi, K.K. (2015). Influence of dust and mud on the optical, chemical, and mechanical properties of a pv protective glass. Sci. Rep. *5*, 15833.

You, S., Lim, Y.J., Dai, Y., and Wang, C.H. (2018). On the temporal modelling of solar photovoltaic soiling: energy and economic impacts in seven cities. Appl. Energy *228*, 1136–1146.

Zorrilla-Casanova, J., Piliougine, M., Carretero, J., Bernaola-Galván, P., Carpena, P., Mora-López, L., and Sidrach-de-Cardona, M. (2012). Losses produced by soiling in the incoming radiation to photovoltaic modules. Prog. Photovolt. Res. Appl. *20*, https://doi.org/10.1002/pip.1258.